# Title: IL-17A controls CNS autoimmunity by regulating gut microbiota and inducing regulatory T cells

**Authors:** Shailesh K. Shahi[1], Sudeep Ghimire[1], Samantha N. Jensen[1,2,†], Peter Lehman[1], Nicholas Borcherding[3], Katherine N. Gibson-Corley[4], Sukirth M. Ganesan[5], Nitin J. Karandikar[1,2,], and Ashutosh K. Mangalam[1,2]*

**Affiliations:**

[1]Department of Pathology, University of Iowa, Iowa City, USA

[2]Graduate Program in Immunology, University of Iowa, Iowa City, USA

[3]Department of Pathology and Immunology, Washington University School of Medicine, Saint Louis, MO,

[4]Department of Pathology, Microbiology & Immunology; Vanderbilt University Medical Center, Nashville, TN

[5]Department of Periodontics College of Dentistry, University of Iowa, Iowa City, USA

† Present address- Department of Microbiology and Immunology, Weill Cornell Medicine, Cornell University, New York, USA

***Corresponding Author**

Ashutosh K. Mangalam, Ph.D.
Department of Pathology,
University of Iowa Carver College of Medicine,
25 S. Grand Avenue, 1080A ML
Iowa City, IA 52242
Phone: 1-319-335-8558
Email. ashutosh-mangalam@uiowa.edu
**ORCID 0000-0002-9926-2531**

**Abstract:** A disrupted equilibrium between IL-17A-producing CD4 T-cells (Th17) and $CD4^+CD25^+FoxP3^+$ regulatory T cells (Tregs) play an important role in the pathobiology of Multiple sclerosis (MS). Gut bacteria help in maintaining immune homeostasis by regulating the balance between anti-inflammatory Tregs and pro-inflammatory Th17 cells. Although, both gut bacteria and Tregs can regulate Th17 cells, the impact of IL-17A on gut microbiota and Tregs is unclear. Utilizing HLA-DR3 transgenic mouse model of MS, we show that IL-17A deficiency (HLA-DR3.IL17A$^{-/-}$ mice) expands Treg-inducing gut bacteria such as *Prevotella*, *Parabacteroides*, and *Bacteroides* and consequently Tregs, resulting in a milder disease in an animal model of MS. Notably, IL-17A sufficient DR3 mice develop milder disease on cohousing with IL-17A-deficient mice, highlighting a dominant role for gut microbiota in inducing Treg and reducing disease severity. Further, we observed an enrichment of bacterial-specific Treg promoting short-chain-fatty-acid metabolic pathways and induction of tolerogenic dendritic cells in HLA-DR3.IL17A$^{-/-}$ mice. Thus, our study shows a novel role of IL-17A in immune homeostasis and inflammation through regulation of the gut microbiota-Treg axis which can be used for the development of gut bacteria as therapeutics for MS.

**Significance of our work**

IL-17A a pro-inflammatory cytokine, is linked with pathobiology of multiple inflammatory diseases including multiple sclerosis (MS) and regulated by both gut microbiota and regulatory CD4 T cells (Tregs). However, the importance of IL-17A in the regulation of gut microbiota and Treg is unknown. Here we show that IL-17A can regulate Treg and disease phenotype by modulating gut microbiota and provide a novel mechanism by which immune-mediators such as IL-17A impact the gut microbiota to alter immune cell function and ultimately disease outcomes. Transfer of milder disease phenotype from IL-17A deficient mice to IL-17A sufficient mice on cohousing indicate a dominant role of gut microbiota in disease suppression. Thus, our study lays the foundation for future studies to unravel the interplay between immunological responses and the gut microbiota which will result in the development of microbiota-based therapeutics to treat autoimmune diseases.

**Main text:**

Multiple sclerosis (MS) is a chronic, inflammatory, neurodegenerative disease of the central nervous system (CNS), in which CD4 T helper (Th) cells of Th1 and/or Th17 phenotype have been shown to play an important role in pathobiology of the disease. IL-17A is a signature pro-inflammatory cytokine of the CD4 T helper 17 (Th17) subset that has emerged as being critical to the pathobiology of MS (1, 2). IL-17A plays a crucial role in resolving extracellular bacterial and fungal infections, by recruiting immune cells, specifically neutrophils, to the site of infection and inducing pro-inflammatory mediators from immune cells as well as fibroblasts, epithelial cells, and endothelial cells (3). However, an aberrant IL-17A response can lead to unresolved inflammation and tissue pathology, as observed in multiple autoimmune diseases including MS (4-7). Thus, although IL-17A is considered a major contributor to the pathogenesis of multiple autoimmune diseases, its precise role in the pathobiology of MS is still being explored. Th17 cells have been shown to be regulated by $CD4^{+}CD25^{+}FoxP3^{+}$ regulatory T cells (Treg) and balance between Treg/Th17 is shown to shift toward Th17 phenotype in inflammatory diseases such as MS (8). Additionally, gut bacteria help in maintaining immune homeostasis by regulating the balance between $CD4^{+}CD25^{+}$FoxP3+ regulatory T cells (Tregs) and pro-inflammatory Th1/Th17 cells (9, 10). The importance of gut microbiota in regulating development of Treg and Th17 is highlighted by studies performed in germ-free mice where absence or reduced Treg and Th17 cells is evident. However, transplant of single bacterium such as segmented filamentous bacterium can restore Th17 (11, 12) and mixture of chloroform resistant *Clostridium* (13) or *Bacteroides fragilis* can induce/restore Treg population in mice (14). These studies highlight an important role of gut microbiota in regulation of Th17 and Treg population and their role in the pathobiology of MS/EAE. However, whether IL-17A can regulate gut microbiota and/or Treg cells is unknown.

In addition to IL-17A, HLA class II genes, specifically HLA-DR2 and -DR3 alleles, are linked as the strongest genetic factors predisposing individuals to MS (15-22). Evidence suggests MS-associated HLA-DR and –DQ alleles regulate disease outcome and severity by modulating pro- and anti-inflammatory cytokine networks (23). Specifically, myelin antigen processed and presented by susceptible HLA-class II molecules such as HLA-DR2, -DR3, or –DR4, can differentiate into Th1 or Th17 secreting cells which can traffic to the CNS and cause neuroinflammation and demyelination, a characteristic of MS (23-27). Thus, HLA class II

transgenic mice have helped in validating the significance of HLA-class II molecules in the pathogenesis of MS (24-28). Additionally, we showed that loss of IFNγ was associated with increased IL-17A levels and severe disease in an HLA-class II transgenic mouse model of experimental autoimmune encephalomyelitis (EAE) (29). Collectively these data suggest that IL-17A might be responsible for severe disease in the absence of IFNγ, however it is unclear whether IL-17A is essential for disease induction or severity or both.

To elucidate the role of IL-17A in the pathogenesis of MS, we generated HLA-DR3 (DR3) class II transgenic mice lacking IL-17A (DR3.IL17A$^{-/-}$) and assessed the outcome on EAE pathogenesis. Mice that express HLA-DR3 were chosen over other EAE models as our prior study suggested a role of IL-17A in disease severity in the absence of IFNγ (30). Unexpectedly, DR3.IL17A$^{-/-}$ transgenic mice were not resistant to EAE, yet developed milder disease compared to IL-17A-sufficient HLA-DR3 transgenic mice. In the absence of IL-17A, interferon-I related gene expression was increased, and CD4$^{+}$CD25$^{+}$FoxP3$^{+}$ Treg were expanded, in part due to enhanced growth of gut bacteria that induce Treg proliferation. The importance of these gut bacteria in modulating IL-17A-mediated disease was confirmed by fecal transplant/cohousing studies. IL-17A-sufficient mice that received fecal transplants from, or that were cohoused with, IL-17A-deficient mice had lower EAE severity relative to IL-17A deficient mice. Bacterial metabolic pathways related to short-chain fatty acid (SCFA) production were enriched in DR3.IL17A$^{-/-}$ transgenic mice. Also, IL10 production from IL-17A deficient mice was higher for both splenic and bone marrow derived dendritic cells suggesting that IL-17A deficiency induces an anti-inflammatory environment. Thus, our study demonstrates that IL-17A regulates Treg levels by modulating the gut microbiota, which alters immune homeostasis and inflammation to promote EAE.

## Results

### IL-17A deficient HLA-class-DR3 transgenic mice develop milder EAE disease

In the HLA class-II transgenic model of EAE, mice lacking IFNγ develop severe brain-specific disease characterized by elevated levels of IL-17A (29). Thus, we hypothesized that in the absence of IL-17A, mice would be resistant to EAE. To investigate the role of IL-17A in EAE, we first generated HLA-DR3 mice as described in Materials and Methods. All transgenic mice developed

normally with no obvious signs of pathology and analysis of splenocytes confirmed these mice lacked IL-17A-expressing $CD4^+$ T cells (Fig. S1).

Interestingly, both DR3 and DR3.IL17A$^{-/-}$ transgenic mice develop EAE disease with similar onset of disease (Fig. 1B). However, DR3.IL17A$^{-/-}$ transgenic mice developed milder disease over time and had a significantly lower cumulative clinical EAE (±) as well as peak EAE score (±) compared to DR3 mice (Fig. 1B, 1C, 1D). Histological analysis of the brain and spinal cord tissues demonstrated milder inflammation and demyelination in DR3.IL17A$^{-/-}$ transgenic mice, consistent with decreased inflammatory cell infiltration in CNS (Fig. 1E, 1F, 1G, 1H). Thus, our data indicate that IL-17A was not required for induction phase of disease. However, the milder disease that occured in the absence of IL-17A over time suggests that it may play a role in disease progression. To test this, we depleted IL-17A in DR3 transgenic mice by treating them with an anti-IL-17A antibody before induction of EAE (Fig. 2). We treated one cohort of mice with the anti-IL-17A antibody prior to immunization with $PLP_{91-110}$, on days -19, -14, -11, -8, and -4 (Fig. 2A). Compared to the control group. DR3 transgenic mice pre-treated with anti-IL-17A still developed EAE however showed a milder disease course which was similar to EAE oberved in DR3.IL17A$^{-/-}$ transgenic mice (Fig. 2B, 2C). Thus, the development of milder disease in DR3 mice in the absence of IL-17A (genetic deficiency as well as IL-17A neutralization) suggests IL-17A is redundent for the induction of disease but might be crucial for disease progression.

To determine if the effect of IL-17A on EAE disease was universal or limited to the HLA class II transgenic mouse model, we assessed the effects of depleting IL-17A in wild-type C57BL/6J (B6) mice. In this mouse strain, EAE was induced with $MOG_{35-55}$ as described previously (31). B6 mice treated with anti-IL-17A antibody after the onset of EAE (i.e., at days 5, 8, 11, 14, 17, 20, 23, 26, 29, and 32 post disease induction) showed significantly lower average clinical scores over time compared to mice treated with PBS or IgG1a (Fig. S2A, 2B). Similar to DR3 transgenic mice, B6 mice that received pre-treatment (i.e., at days -24,-21,-18,-15,-12,-9,-6, and -3) and post-treatment (days 5, 8, 11, 14, and 17) of anti-IL-17A antibody still developed EAE but exhibited lower disease severity (Fig. S2C, 2D). These data indicated that the IL-17A is redundent for disease induction both in PLP-DR3-EAE and MOG-B6-EAE models. to exacerbate EAE progression occurs in both HLA-DR3 transgenic and wild-type B6 mice, and is not limited to one model of disease.

Even though IL-17A is considered as an important cytokine for the development of EAE (32), our results suggest that IL-17A is more crucial for disease progression. Further, the development of EAE disease in the absence of IL-17A, suggests IL-17A is not essnetial for development of EAE and other inflammatory cytokines might compensate for IL-17A to induce disease. The potential candidates are IL-17F, GM-CSF and IFNγ as they have been shown to play an important role in EAE disease. As IL-17F share 55% homology at the amino acid level with IL-17A, and may compensate for IL-17A , we analyzed the levels of IL-17F and found that IL-17A deficient mice have significantly higher levels of the IL-17F compared to IL-17A sufficient DR3 mice (Fig. S3). However, neutralization of IL-17F had no effect on disease incidence or severity (Fig. S4A, 4B). Next, we investiagted whether GM-CSF was compensating for EAE induction in IL-17A deficient mice, as GM-CSF is shown to be a pathogenic cytokine in EAE (33). Although antigen specific CD4 T cells from DR3.IL17A$^{-/-}$ transgenic mice did not show increased levels of GM-CSF but neutralization of the GM-CSF in DR3.IL17A$^{-/-}$ resulted in increased average disease score at later point of the disease (Fig. S4A, S4B). However, the cumulative disease score was similar between isotype control and anti-GM-CSF treated mice (Fig. S4C). Thus, our data suggested that both GM-CSF and IL-17F did not compensate for IL-17A in DR3.IL-17A$^{-/-}$ transgenic mice for disease induction (Fig. S4). To determine the role of IFNγ in disease progression, we generated DR3 transgenic mice in which both IFNγ and IL-17A were deleted (DR3.IL17A$^{-/-}$IFNγ$^{-/-}$). Interestingly, these mice still developed disease similar to that observed in DR3 transgenic mice (Fig. S5) suggesting that neither IL-17A nor IFNγ is required for the development of EAE disease. Taken together, our data indicate that neither IL-17A nor IL-17For GM-CSF, or IFNγ are required for the development of EAE disease. Thus, our data point toward an inflammatory mediator besides IL-17A, IL-17F, IFNγ or GM-CSF in the induction of EAE disease.

**IL-17A deficiency enhances proliferation of CD4$^{+}$CD25$^{+}$FOXP3$^{+}$ Treg cells**

The milder course of EAE disease observed in IL-17A-deficient mice suggested the possibility of an immune-regulatory mechanism at play to dampen the chronic immune response. Studies have shown that CD4$^{+}$CD25$^{+}$Foxp3$^{+}$ regulatory T cells can regulate autoimmune inflammation in the body and suppress IL-17A-secreting CD4+ Th17 cells (34, 35). However, few studies have examined the ability of IL-17A to modulate Treg. Therefore, we analyzed the total number of

$CD4^+CD25^+Foxp3^+$ regulatory T cells in peripheral blood of DR3 and DR3.IL17A$^{-/-}$ transgenic mice. We observed that DR3.IL-17A$^{-/-}$ transgenic mice had a significantly higher percentage (Fig. 3A, 3B) and number (Fig. 3C) of $CD4^+CD25^+Foxp3^+$ regulatory T cells compared to DR3 transgenic mice. To determine whether the increased Treg levels were responsible for milder disease phenotype in DR3.IL17A$^{-/-}$ transgenic mice, we treated these mice with an anti-CD25 blocking antibody to neutralize the Treg population as shown in Fig 3D (36). CD25 neutralization in DR3.IL17A$^{-/-}$ transgenic mice resulted in severe disease phenotype similar to DR3 transgenic mice, indicating that Treg were involved in establishing milder disease phenotype in DR3.IL17A$^{-/-}$ transgenic mice (Fig. 3E). Notably, $CD4^+CD25^+$ Treg that were isolated from the spleen of naïve DR3.IL17A$^{-/-}$ transgenic mice had significantly higher suppressive ability against antigen specific $CD4^+CD25^-$ effector cells when compared to those of DR3 transgenic mice (Fig. 3F), further supporting the role of Treg in determining clinical EAE outcomes in DR3.IL17A$^{-/-}$ transgenic mice. Collectively, our data indicate that deficiency of IL-17A results in a higher frequency and number of $CD4^+CD25^+$ Treg cells with a higher suppressive ability, which likely contributes to a milder disease phenotype in DR3.IL-17A$^{-/-}$ transgenic mice.

**Loss of IL-17A enriched interferon-I-related genes in the colon of DR3 transgenic mice**

The majority of immune population reside near mucosal surfaces specifically in the gut to protect large surface area. Trillions of bacteria (microbiota) living in the gut specifically in the colon had been shown to play an important role in the generation of Treg and Th17 cells. The importance of gut microbiota in generation of Treg is highlighted by studies performed in germ-free/antibiotic treated mice, which showed significantly reduced Treg population (37, 38). Interestingly, colonization of germ-free/antibiotic treated mice with specific commensals can restore Treg population and function (37-39).

Therefore, to identify whether the genes that might be involved in modulating the disease in IL-17A deficient transgenic mice, we collected the colonic tissues from both DR3 and DR3.IL17A-/- transgenic mice before inducing EAE and performed transcriptome analysis (Fig. 4A). We observed that the colonic tissues from mice of the different genotype (e.g., DR3 and DR3.IL17A$^{-/-}$) were distinctly separated (Fig. 4B). Upon differential analysis, we identified 123 genes that were differentially expressed in the colon between the two groups (Fig. 4C, 4D, Table S1). Thirty-three out of 123 differentially expressed genes were upregulated in DR3.IL17$^{-/-}$ transgenic mice relative

to DR3 transgenic mice. This included genes in the following GO functional categories: *immune function*, *immune effector process*, and *immune system process* (*Oasl2*, *Oas3*, and *Cfd*), *activation of the immune response*, *regulation of immune system process*, and *immune response* (*Cfd*), *signaling* (*Cfd*), and *response to stimulus* (*Oasl2*, *Oas3*, *Cfd*, *Fabp4*, and *Ifit3*). Majority of these genes belong to type-I interferon category and are shown to be involved in anti-inflammatory responses (40). The induction of type I interferon genes (e.g., *Oas*-like proteins, *Ifit3*) have been associated with the stability and function of Treg under stress conditions and promotes induction of IL-10 expression to enhance their suppressive ability (41, 42). In addition, 90 genes were downregulated in DR3.IL17$^{-/-}$ transgenic mice relative to DR3 transgenic mice (Fig. 4C, 4D, Table S1), of which only *Ccl28* was related to immune function and was identified in the GO categories *immune system process* and *immune response*. Thus, our observation of enrichment of type-I interferon genes in the colon of DR3.IL17A$^{-/-}$ transgenic mice suggested that these changes may contribute to the difference in disease phenotype between DR3 and DR3.IL17A$^{-/-}$ transgenic mice specifically the ability of type-1 IFN to induce Tregs.

**IL-17A deficiency modulates the composition of the gut microbiome**

The enhancement of Treg and type-I interferon genes in DR3.IL17A$^{-/-}$ transgenic mice relative to DR3 transgenic mice prompted us to investigate the changes in the composition and function of the gut microbiota that might impact the immune response. As gut microbiome is known to modulate the Treg, first, we hypothesized that absence of IL-17A modulated the composition of the gut microbiome which then can induce Treg population and leading to milder disease phenotype in DR3.IL17A$^{-/-}$ transgenic mice. Secondly, we hypothesize that the microbiota enriched in IL-17A deficient mice when transferred to IL-17A sufficient mice should alter the microbiota of DR3 transgenic mice to enhance Treg in the gut.

To test our first hypothesis i.e., if IL-17A could alter gut microbiota, we collected fecal samples from both DR3 and DR3.IL17A$^{-/-}$ transgenic mice before cohousing and performed shotgun metagenomic sequencing to characterize the microbiome in these mice (Fig 5A). The microbial composition of DR3 transgenic mice clustered distinctly from that of DR3.IL17A$^{-/-}$ transgenic mice (Fig. S6). Specifically, we observed a significant increase in the average relative abundance of *Prevotella* sp. MGM1, *Parabacteroides distasonis*, and *Bacteroides sartorii* in DR3.IL17A$^{-/-}$

transgenic mice (Fig. 5B, 5C, 5D, 5E). We did observe that DR3.IL17A$^{-/-}$ transgenic mice had a significant reduction in the population of *B. vulgatus*, *Lachnospiraceae* bacterium 10_1, *Lachnospiraceae* bacterium 28_4, *Lachnospiraceae* bacterium COE1, and *Lachnospiraceae* bacterium A2 (Fig. 5F, 5G, 5H, 5I, 5J). A complete list of bacteria showing trend but not reaching statistical significance have been provided in Figure S7.

For efficient microbiota transfer we first performed fecal transplantation through oral gavage followed by cohousing as described previously (43, 44) . We next analyzed the microbiota of DR3.IL17A$^{-/-}$ and DR3 transgenic mice after fecal transplantation/cohousing and observed that the microbial composition in DR3 transgenic mice shifted to become more similar to that in DR3.IL17A$^{-/-}$ transgenic mice (Fig. 5B, Fig. S6). Specifically, *Prevotella* sp. MGM2 (Fig. 5K) and *E. coli* (Fig. 5L) were significantly increased in DR3 transgenic mice after cohousing with DR3.IL17A$^{-/-}$ transgenic mice. *Prevotella* species were observed to be significantly higher in DR3.IL17A$^{-/-}$ transgenic mice compared to DR3 transgenic mice prior to cohousing too and especially *Prevotella* sp. MGM2 had significantly higher relative abundance in DR3 transgenic mice after being cohoused with DR3.IL17A$^{-/-}$ transgenic mice. Also, *A. muciniphila*, and *H. typhlonius* were absent in DR3 transgenic mice before they were cohoused but were increased but not significantly after cohousing with DR3.IL17A$^{-/-}$ transgenic mice (Fig. 5B, Fig. S7). Similarly, the abundance of *Prevotella* sp. MGM1, *P. distasonis* and *B. sartorii* were increased, although not to significant levels, in DR3 transgenic mice after being cohoused with DR3.IL17A$^{-/-}$ transgenic mice (Fig. 5C, 5D, 5E). In contrast, *Lachnospiraceae* bacterial species (Fig. 5G, 5I and 5J) and *Muribaculaceae* bacterium DSM 10370 (Fig. 5M) were significantly decreased in DR3 transgenic mice after being cohoused with DR3.IL17A$^{-/-}$ transgenic mice. Thus, the cohousing of DR3 transgenic mice with DR3.IL1-17A$^{-/-}$ transgenic mice transformed microbiota in DR3 mice so that bacteria that are supportive of Treg were expanded, whereas those that diminished Treg function were decreased.

**Cohousing DR3 mice with DR3.IL17A$^{-/-}$ transgenic mice transfers a Treg-inducing phenotype**

As deficiency of IL-17A was associated with alterations in the composition of the gut microbiota and Treg numbers and fecal transplantation plus cohousing resulted in successful colonization by

microbial species from IL-17A deficient mice to IL-17A sufficient mice, we hypothesized that transferring the gut microbiome from DR3.IL17A$^{-/-}$ transgenic mice to DR3 transgenic mice would also increase Treg frequency and subsequently reduce EAE severity in recipients. Therefore, we assessed the levels of CD4$^{+}$CD25$^{+}$FoxP3$^{+}$ Treg cells present in the peripheral blood for both IL-17A deficient and IL-17A sufficient transgenic mice after fecal transplantation plus cohousing (Fig. 6A). We observed that CD4$^{+}$CD25$^{+}$FoxP3$^{+}$ T cell populations were significantly increased in DR3 transgenic mice that received a combination of fecal transplants plus cohousing with DR3.IL17A$^{-/-}$ transgenic mice (Fig. 6B). In contrast, these Treg populations were similar in DR3.IL17A$^{-/-}$ transgenic mice that received fecal transplants from DR3 transgenic both before and after the mice were cohoused (Fig. 6C). These data suggest that microbes transferred from DR3.IL17A$^{-/-}$ transgenic mice to DR3 transgenic mice, followed by cohousing, were crucial to enhance the Treg population.

As the transfer of microbiota from DR3.IL17A$^{-/-}$ transgenic mice to DR3 transgenic mice increased the Treg population (Fig. 6B, 6C), we sought to examine if these changes also affected the outcome of EAE disease phenotype. DR3 and DR3.IL17A$^{-/-}$ transgenic mice were cohoused for four weeks and then housed separately while EAE was induced, and the course of disease was assessed. When housed separately DR3 transgenic mice showed severe disease compared to DR3.IL17A$^{-/-}$ transgenic mice as expected (Fig. 6D, 6E). In contrast, DR3 transgenic mice that were cohoused with DR3.IL17A$^{-/-}$ transgenic mice showed milder disease compared to DR3 control mice that were never cohoused (Fig 6D, 6E). However, the disease in DR3.IL-17$^{-/-}$ transgenic mice were similar pre and post-cohousing with DR3 transgenic mice. Thus, our results confirmed that the lack of IL-17A alters the composition of the gut microbiota to allow the expansion of bacteria such as *Prevotella* sp. MGM2, leading to the expansion of the Treg population and ultimately, to milder EAE disease phenotype.

**Short-chain fatty acid metabolic pathways are transferred from DR3.IL17A$^{-/-}$ transgenic mice to DR3 transgenic mice after cohousing.**

Next to identify the mechanism through which IL-17A influenced gut microbiota can modulate Treg, we compared bacterial metabolic pathways enriched in DR3.IL-17A$^{-/-}$ mice. We first assessed short-chain fatty acids (SCFAs), as these have been previously reported to affect the

differentiation of T cells (45) and ameliorate EAE severity (46). The metabolic pathways associated with pyruvate to propanoate (P108-PWY) and pyruvate fermentation to acetate and lactate II (PWY-5100) trended higher, although not to significant levels, in DR3.IL17A$^{-/-}$ transgenic mice compared to DR3 transgenic mice before cohousing. P108-PWY was low in abundance in both DR3 and DR3.IL17A$^{-/-}$ transgenic mice before cohousing but was significantly higher in both strains after cohousing (Fig. S8A). Likewise, pyruvate fermentation to acetate and lactate II was lower in DR3 transgenic mice but became significantly enriched after mice were cohoused with DR3.IL17A$^{-/-}$ transgenic mice (Fig. S8B). The transfer of SCFA pathways from DR3.IL17A$^{-/-}$ transgenic mice to DR3 transgenic mice, but not vice versa, indicates that the DR3.IL17A$^{-/-}$ transgenic mice harbor microbes that are responsible for SCFAs production and these microbes can be transferred to DR3 transgenic mice through co-housing. Thus, our data suggest the potential role of bacterial SCFAs in inducing Treg to produce milder disease in the absence of IL-17A.

**Dendritic cells in DR3.IL17A$^{-/-}$ transgenic mice produce higher levels of IL-10**

SCFAs such as butyrate and propionate can exhibit strong anti-inflammatory effects by inhibiting expression of IL-6, IL-12 and IL-23 from dendritic cells (DCs) (47). Butyrate and propionate also suppress lipopolysaccharide (LPS)-induced DC activation (48). As bacterial metabolic pathway analysis showed a significant increase in the number of propionate I production pathway, we hypothesized that higher levels of SCFAs in the gut will alter DCs phenotype and make them tolerogenic. Therefore, we analyzed the production of the anti-inflammatory cytokine, IL-10, from DCs in naïve DR3 and DR3.IL17A$^{-/-}$ transgenic mice that were stimulated with LPS. Interestingly, CD11c$^{+}$ DCs from naïve DR3.IL17A$^{-/-}$ transgenic mice produced significantly higher levels of IL-10 compared to DR3 transgenic mice after stimulation with LPS (Fig. 7A). Similarly, bone marrow-derived DCs from DR3.IL17A$^{-/-}$ transgenic mice produced significantly higher levels of IL-10 when compared to DR3 transgenic mice (Fig. 7B). Finally, analysis of antigen presentation capacity showed that bone marrow-derived DCs from DR3.IL17A$^{-/-}$ transgenic mice had a reduced ability to induce antigen-specific CD4$^{+}$ T cell proliferation compared to DR3 transgenic mice (Fig. 7C). Thus, our data suggests CD11c+ DC from DR3.IL17A$^{-/-}$ transgenic mice adopted a tolerogenic phenotype characterized by higher levels of IL-10 with reduced antigen presentation

capacity. Therefore, this phenotype suggests CD11c+ DCs may be involved in limiting disease severity in DR3.IL17A$^{-/-}$ transgenic mice.

## Discussion

The ability of IL-17A to influence autoimmune diseases has been well established but the precise mechanism by which this occurs is poorly understood. In this study, we show that IL-17A is critical for regulating EAE disease progression through its ability to modulate the gut microbiota and alter the number and function of Treg. Although not required for disease initiation, our work shows that IL-17A regulates disease severity by suppressing the Treg population through depletion of Treg-promoting bacteria. This protective effect of gut microbiota was transferable as cohousing of IL-17A sufficient DR3 transgenic with DR3.IL17A$^{-/-}$ transgenic mice resulted in gut microbiota profile, Treg phenotype and milder disease similar to DR3.IL17A$^{-/-}$ transgenic mice. Thus, our data identify an important pathway through which an immune-mediated cytokine modulates the gut microbiota to influence the course of inflammatory diseases such as MS.

The development of milder disease in DR3.IL17A$^{-/-}$ transgenic mice suggests induction of regulatory pathways in the absence of IL-17A. In support of this, we observed an increase in the CD4$^{+}$CD25$^{+}$FoxP3$^{+}$ Treg population in DR3.IL17A$^{-/-}$ transgenic mice. Further, disease was restored after Treg depletion using anti-CD25 (PC61) antibody, confirming an important role for CD4+CD25+ Treg subset in disease regulation. Interestingly, similar observation had been also reported in GM-CSF deficient mice which are resistant to EAE development but treatment with anti-CD25 antibody (PC61) resulted in the development of severe disease (49). Thus, these data suggests that pathogenic cytokine such as IL-17A and GM-CSF might influence EAE disease progression through downregulation of regulatory cells such as CD4$^{+}$CD25$^{+}$ Treg cells. Development of disease in mice lacking IL-17A or mice receiving CD4$^{+}$ T cells from *Csf2*-/- (mice lacking GM-CSF) support our argument that neither IL-17A nor GM-CSF are essential for disease development in EAE model.

In recent years, gut microbiota has emerged as an important factor in the induction and regulation of both Treg and Th17 cell subsets (38). However, effect of IL-17A on gut microbiome is poorly understood and it has been suggested that IL-17A/F can act as modulators of intestinal homeostasis

(50). Therefore, we hypothesized that the absence of IL-17A enables the expansion of certain species in the gut microbiota that are responsible for the induction of Treg. The presence of distinct microbiota profiles between DR3 and DR3.IL17A$^{-/-}$ transgenic mice strengthen our hypothesis. Specifically, we observed an expansion of gut bacteria that are known to promote the Treg population, including *Prevotella* species, *Parabacteroides distasonis* and *Bacteroides species* (9, 51-53). Of these species, *Prevotella* sps. MGM2 successfully transferred to the IL-17A sufficient mice from IL-17A deficient mice in high numbers. At the same time, the abundances of none of the microbial species were affected significantly in IL-17A deficient mice after cohousing with IL-17A sufficient mice suggesting that the microbial ecosystem of DR3.IL17A$^{-/-}$ transgenic mice prior to cohousing was at higher stable state compared to DR3 transgenic mice. Also, the microbial community of DR3 transgenic mice which clustered separately from DR3.IL17A$^{-/-}$ transgenic mice before fecal transplant and cohousing were clustering with DR3.IL17A$^{-/-}$ transgenic mice after fecal transplant and cohousing (Fig. S6) indicating that microbial composition of DR3.IL17A$^{-/-}$ transgenic mice were resilient to change compared to DR3 transgenic mice. Ecologically, the degree of resistance of the microbiota against incoming microbial species is crucial in determining health and disease (54). The lower stability and the loss of resistance of the gut microbiota in DR3 transgenic mice was ultimately reflected by exacerbated disease severity, which was reduced upon cohousing with DR3.IL17A$^{-/-}$ transgenic mice, suggesting that the gut microbiota of DR3 transgenic mice was re-configured to restore its protective functions. In particular, cohousing IL-17A-deficient mice with IL-17A sufficient mice resulted in the transfer of crucial Treg-stimulating bacteria, such as *Prevotella* species into IL-17A sufficient DR3 transgenic mice. Indeed, introducing *Prevotella* species can reduce the severity of EAE due to changes in the gut microbiota that ultimately induce Treg (51, 52). Taken together, our study demonstrates gut microbiota dependent internal mechanism to maintain intestinal homeostasis and Treg function and perturbation of the same can promote inflammation and CNS autoimmunity. Suppression of disease in IL-17A sufficient mice on cohousing with IL-17A deficient mice strongly suggest that Treg promoting gut microbiota is dominant over disease promoting bacteria and thus have strong clinical translation potential. However, the microbial community network and the interplay between the microbes in the community to exacerbate or protect from EAE warrants deeper exploration.

SCFAs are produced by the gut microbiota through anaerobic fermentation of polysaccharides and are involved in enhancing IL-10 production and are crucial for maintaining gut homeostasis (55). Oral administration of a lactate-producing bacterium *P. acidilactici* suppressed EAE by inducing IL-10-producing Treg (56). In addition, SCFAs maintain the integrity of the gut barrier (57) and blood-brain barrier (BBB) in the CNS (58, 59). Correspondingly, germ-free mice have reduced expression of tight junction proteins, such as occludin and claudin, in the BBB, an effect that increases with age. Recolonization of these mice with diverse microbiota increases the integrity of both gut and the BBB (60). We have previously shown that mice with EAE have leaky gut and BBB, however treatment with *Prevotella* restored both gut and blood brain barrier (51). The lower abundance of these SCFAs pathways in DR3 transgenic mice compared to DR3.IL17A$^{-/-}$ transgenic mice indicate that in the presence of IL-17A, there is a decreased abundance of microbial populations with the capability to produce SCFAs. However, cohousing of DR3 transgenic mice with DR3.IL17$^{-/-}$ transgenic mice restored microbial SCFA pathways involved in propionate, acetate, and lactate production. Propionate had been shown to decrease the differentiation of Th17 cells and enhance the differentiation of Treg (45, 61). Also, the significant rise in pyruvate fermentation to propionate I (P108-PWY) and pyruvate fermentation to acetate and lactate II (PWY-5100) in DR3 transgenic mice after being cohoused with DR3.IL17A$^{-/-}$ transgenic mice suggests that the transfer of microbial metabolic pathways can alter immune cell functions and consequently disease outcome. Thus, absence of IL-17A resulted in the enrichment of gut bacteria with ability to produce SCFA which then can modulate disease through induction of Treg.

The majority of Treg that are induced by gut bacteria are found in the colon. Therefore, we performed gene expression analysis of the colon of IL-17A-sufficient and -deficient DR3 transgenic mice to determine the differentially expressed genes which might be important for reduced severity of disease phenotype in IL-17A deficient mice. Interestingly, IL-17A-deficient mice, which exhibit an enhanced Treg population and altered gut microbiota composition, showed increased expression of type I interferon genes. Genes belonging to type-I interferon categories are indicated as important mediators of anti-inflammatory responses (40). Indeed, type I interferon genes are previously known to promote the suppressive ability of Treg (41, 42). Although IL-17A deficiency had no effect on the Treg population in a previous study that utilized both IL-17A and

IL-17F (50), we report that the levels of $CD4^{+}CD25^{+}FoxP3^{+}$ T cell populations were significantly higher in the DR3.IL17A$^{-/-}$ transgenic mice compared to DR3 transgenic mice. Thus, the induction of Treg in the colon in the absence of IL-17A is likely critical for regulating inflammation in the context of EAE.

Next, the induction of Treg in IL-17A deficient mice was concurrent with the increased production of IL-10 from splenic dendritic cells in naïve, immunized DR3.IL17A$^{-/-}$ transgenic mice. It suggested that the tolerogenic DCs are induced in the absence of IL-17A and DC-derived IL-10 is essential to ameliorate EAE severity (62). The reduced antigen presentation capacity of DCs from DR3.IL17A$^{-/-}$ transgenic mice further support a role of tolerogenic DCs in mice lacking IL-17A. SCFAs such as propionate and butyrate have been demonstrated as potent inducers of tolerogenic DCs previously (48). Thus, it is possible that SCFAs produced by the gut microbiota in the current study could have induced tolerogenic DCs in IL-17A deficient mice, however, details of how the gut microbiota affect DC proliferation and prompt IL-10 production are only beginning to be investigated.

Finally, we observed that IL-17A significantly affects disease progression without affecting the onset of disease. This is consistent with other studies such as Haak et al., who showed that either loss of IL-17A or overexpression of IL-17A in CNS has a major impact on disease development (63). It is possible that other Th17 (IL-17F and GM-CSF) or even Th1 cytokine (IFNγ) can compensate for IL-17A loss for disease development. However, in our study, mice that were treated with blocking antibodies against IL-17F or GM-CSF still developed disease. IL-17F is a member of the IL-17 family of cytokines, a number of studies have investigated its role in EAE, however the majority of studies have concluded that IL-17F is either redundant or don’t play a role in EAE model (63, 64). IL-17F deficient mice treated with anti-IL-17A blocking antibodies were susceptible to EAE (63). The role of GM-CSF in EAE and MS is still matter of debate, with some studies suggesting it is essential for EAE disease as GM-CSF deficient mice are resistant to EAE development (65) whereas others have shown that GM-CSF is not essential for EAE development (33, 66). Interestingly, Duncker et al., observed that although GM-CSF is required for disease progression, it was dispensable for disease induction phase (33). Development of severe disease in DR3 mice lacking both IL-17A and IFNγ ruled out a role of IFNγ in disease induction in the

absence of IL-17A. Thus, our data suggest that IL-17A together with IL-17F, GM-CSF or IFNγ, is dispensable for disease induction phase as DR3.IL-17A$^{-/-}$ transgenic mice still develop disease, although a milder course. Future studies will be necessary to determine the mechanisms driving disease in the absence of IL-17A.

Our results have strong clinical relevance as modulation of the gut microbiota are being considered as potential therapeutics to treat diseases ranging from inflammatory to neurological diseases. As MS is an inflammatory disease characterized by gut dysbiosis, combination therapies targeted to reduce inflammation as well as correct gut dysbiosis might results in better therapeutic outcome than either one alone. Although IL-17A had been linked with the pathobiology of MS, two anti-IL17A clinical trials in MS (NCT01874340 and NCT01433250) were terminated early. In that regard, while anti-IL-17A therapy alone did not prove as effective as current MS drugs, combination of anti-IL-17A and microbiota modulation might provide better therapeutic efficacy. Additionally, Treg induction is also being tried as potential treatment option in MS (67). Our cohousing experiment showing ability of gut microbiota to colonize, induce Tregs and suppress disease in susceptible mice suggests that gut microbiota-based induction of host immunity might have added advantage as it will not only induce Tregs but can correct gut dysbiosis too. Future studies testing gut commensal with Treg inducing capabilities in combination with anti-IL-17A are warranted to test whether a combination of anti-inflammatory plus gut commensal modulation might provide added benefits.

In summary, our study highlights an important pathway through which IL-17A regulates inflammation, specifically by modulating the gut microbiota to suppress Treg expansion. Most notably, our data show that the Treg inducing gut microbiota from DR3.IL17A$^{-/-}$ can transfer disease protection to DR3 transgenic mice to reduce disease severity and progression. In the absence of IL-17A, the gut microbiota appears stable and resilient to changes in its composition compared to IL-17A sufficient mice. Thus, our study illuminates a novel mechanism by which immune-mediators such as cytokines impact the gut microbiota to alter immune cell function and ultimately disease outcomes and lays the foundation for future studies that unravel the interplay between immunological responses and the gut microbiota provides long-term implications for the development of microbiota-based therapeutics to treat autoimmune diseases.

## References


1. T. Korn, E. Bettelli, M. Oukka, V. K. Kuchroo, IL-17 and Th17 Cells. *Annual review of immunology* **27**, 485-517 (2009).
2. J. Milovanovic *et al.*, Interleukin-17 in Chronic Inflammatory Neurological Diseases. *Front Immunol* **11**, 947 (2020).
3. M. M. Curtis, S. S. Way, Interleukin-17 in host defence against bacterial, mycobacterial and fungal pathogens. *Immunology* **126**, 177-185 (2009).
4. W. P. Chong *et al.*, The Cytokine IL-17A Limits Th17 Pathogenicity via a Negative Feedback Loop Driven by Autocrine Induction of IL-24. *Immunity* **53**, 384-397 e385 (2020).
5. P. S. Biswas, IL-17 in Renal Immunity and Autoimmunity. *J Immunol* **201**, 3153-3159 (2018).
6. Y. Iwakura, S. Nakae, S. Saijo, H. Ishigame, The roles of IL-17A in inflammatory immune responses and host defense against pathogens. *Immunological reviews* **226**, 57-79 (2008).
7. M. J. McGeachy, D. J. Cua, S. L. Gaffen, The IL-17 Family of Cytokines in Health and Disease. *Immunity* **50**, 892-906 (2019).
8. B. M. Segal, Stage-specific immune dysregulation in multiple sclerosis. *J Interferon Cytokine Res* **34**, 633-640 (2014).
9. K. M. Nutsch, C. S. Hsieh, T cell tolerance and immunity to commensal bacteria. *Curr Opin Immunol* **24**, 385-391 (2012).
10. C. T. Weaver, R. D. Hatton, Interplay between the TH17 and TReg cell lineages: a (co-)evolutionary perspective. *Nat Rev Immunol* **9**, 883-889 (2009).
11. Y. Yang *et al.*, Focused specificity of intestinal TH17 cells towards commensal bacterial antigens. *Nature* **510**, 152-156 (2014).
12. Ivanov, II *et al.*, Induction of intestinal Th17 cells by segmented filamentous bacteria. *Cell* **139**, 485-498 (2009).
13. K. Atarashi *et al.*, Treg induction by a rationally selected mixture of Clostridia strains from the human microbiota. *Nature* **500**, 232-236 (2013).
14. K. M. Telesford *et al.*, A commensal symbiotic factor derived from Bacteroides fragilis promotes human CD39(+)Foxp3(+) T cells and Treg function. *Gut Microbes* **6**, 234-242 (2015).
15. C. Alvarado-de la Barrera *et al.*, HLA class II genotypes in Mexican Mestizos with familial and nonfamilial multiple sclerosis. *Neurology* **55**, 1897-1900 (2000).
16. L. F. Barcellos *et al.*, HLA-DR2 dose effect on susceptibility to multiple sclerosis and influence on disease course. *American journal of human genetics* **72**, 710-716 (2003).
17. G. C. DeLuca *et al.*, An extremes of outcome strategy provides evidence that multiple sclerosis severity is determined by alleles at the HLA-DRB1 locus. *Proceedings of the National Academy of Sciences of the United States of America* **104**, 20896-20901 (2007).
18. D. A. Dyment *et al.*, Complex interactions among MHC haplotypes in multiple sclerosis: susceptibility and resistance. *Human molecular genetics* **14**, 2019-2026 (2005).
19. J. R. Oksenberg *et al.*, Mapping multiple sclerosis susceptibility to the HLA-DR locus in African Americans. *American journal of human genetics* **74**, 160-167 (2004).
20. O. Olerup, J. Hillert, HLA class II-associated genetic susceptibility in multiple sclerosis: a critical evaluation. *Tissue antigens* **38**, 1-15 (1991).
21. S. V. Ramagopalan *et al.*, Analysis of 45 candidate genes for disease modifying activity in multiple sclerosis. *J Neurol* **255**, 1215-1219 (2008).
22. S. V. Ramagopalan *et al.*, The inheritance of resistance alleles in multiple sclerosis. *PLoS genetics* **3**, 1607-1613 (2007).

539 23. A. K. Mangalam, V. Taneja, C. S. David, HLA class II molecules influence susceptibility versus
540 protection in inflammatory diseases by determining the cytokine profile. *Journal of immunology*
541 **190**, 513-518 (2013).
542 24. N. Kaushansky, A. Ben-Nun, DQB1*06:02-Associated Pathogenic Anti-Myelin Autoimmunity in
543 Multiple Sclerosis-Like Disease: Potential Function of DQB1*06:02 as a Disease-Predisposing
544 Allele. *Front Oncol* **4**, 280 (2014).
545 25. J. Klehmet *et al.*, T cell epitope spreading to myelin oligodendrocyte glycoprotein in HLA-DR4
546 transgenic mice during experimental autoimmune encephalomyelitis. *Clin Immunol* **111**, 53-60
547 (2004).
548 26. J. A. Quandt *et al.*, Myelin basic protein-specific TCR/HLA-DRB5*01:01 transgenic mice support
549 the etiologic role of DRB5*01:01 in multiple sclerosis. *J Immunol* **189**, 2897-2908 (2012).
550 27. S. A. Nalawade *et al.*, Aire is not essential for regulating neuroinflammatory disease in mice
551 transgenic for human autoimmune-diseases associated MHC class II genes HLA-DR2b and HLA-
552 DR4. *Cellular immunology* **331**, 38-48 (2018).
553 28. D. Luckey, D. Bastakoty, A. K. Mangalam, Role of HLA class II genes in susceptibility and resistance
554 to multiple sclerosis: studies using HLA transgenic mice. *J Autoimmun* **37**, 122-128 (2011).
555 29. A. K. Mangalam *et al.*, Absence of IFN-gamma increases brain pathology in experimental
556 autoimmune encephalomyelitis-susceptible DRB1*0301.DQ8 HLA transgenic mice through
557 secretion of proinflammatory cytokine IL-17 and induction of pathogenic monocytes/microglia
558 into the central nervous system. *J Immunol* **193**, 4859-4870 (2014).
559 30. A. Mangalam *et al.*, HLA-DQ6 (DQB1*0601)-restricted T cells protect against experimental
560 autoimmune encephalomyelitis in HLA-DR3.DQ6 double-transgenic mice by generating anti-
561 inflammatory IFN-gamma. *J Immunol* **180**, 7747-7756 (2008).
562 31. S. N. Jensen *et al.*, Isoflavone diet ameliorates experimental autoimmune encephalomyelitis
563 through modulation of gut bacteria depleted in patients with multiple sclerosis. *Sci Adv* **7** (2021).
564 32. Y. Komiyama *et al.*, IL-17 plays an important role in the development of experimental autoimmune
565 encephalomyelitis. *J Immunol* **177**, 566-573 (2006).
566 33. P. C. Duncker, J. S. Stoolman, A. K. Huber, B. M. Segal, GM-CSF Promotes Chronic Disability in
567 Experimental Autoimmune Encephalomyelitis by Altering the Composition of Central Nervous
568 System-Infiltrating Cells, but Is Dispensable for Disease Induction. *J Immunol* **200**, 966-973 (2018).
569 34. Z. Li, D. Li, A. Tsun, B. Li, FOXP3+ regulatory T cells and their functional regulation. *Cell Mol*
570 *Immunol* **12**, 558-565 (2015).
571 35. S. Hori, T. Nomura, S. Sakaguchi, Control of regulatory T cell development by the transcription
572 factor Foxp3. *Science* **299**, 1057-1061 (2003).
573 36. A. D. Christensen, S. Skov, P. H. Kvist, C. Haase, Depletion of regulatory T cells in a hapten-induced
574 inflammation model results in prolonged and increased inflammation driven by T cells. *Clin Exp*
575 *Immunol* **179**, 485-499 (2015).
576 37. K. Atarashi *et al.*, Induction of colonic regulatory T cells by indigenous Clostridium species. *Science*
577 **331**, 337-341 (2011).
578 38. J. L. Round, S. K. Mazmanian, Inducible Foxp3+ regulatory T-cell development by a commensal
579 bacterium of the intestinal microbiota. *Proceedings of the National Academy of Sciences of the*
580 *United States of America* **107**, 12204-12209 (2010).
581 39. M. B. Geuking *et al.*, Intestinal bacterial colonization induces mutualistic regulatory T cell
582 responses. *Immunity* **34**, 794-806 (2011).
583 40. E. N. Benveniste, H. Qin, Type I interferons as anti-inflammatory mediators. *Sci STKE* **2007**, pe70
584 (2007).
585 41. C. A. Stewart *et al.*, Interferon-dependent IL-10 production by Tregs limits tumor Th17
586 inflammation. *J Clin Invest* **123**, 4859-4874 (2013).

587 42. L. Zhang, S. Yuan, G. Cheng, B. Guo, Type I IFN promotes IL-10 production from T cells to suppress
588 Th17 cells and Th17-associated autoimmune inflammation. *PLoS One* **6**, e28432 (2011).
589 43. T. L. Montgomery *et al.*, Interactions between host genetics and gut microbiota determine
590 susceptibility to CNS autoimmunity. *Proceedings of the National Academy of Sciences of the*
591 *United States of America* **117**, 27516-27527 (2020).
592 44. V. K. Ridaura *et al.*, Gut microbiota from twins discordant for obesity modulate metabolism in
593 mice. *Science* **341**, 1241214 (2013).
594 45. A. Haghikia *et al.*, Dietary Fatty Acids Directly Impact Central Nervous System Autoimmunity via
595 the Small Intestine. *Immunity* **43**, 817-829 (2015).
596 46. M. Mizuno, D. Noto, N. Kaga, A. Chiba, S. Miyake, The dual role of short fatty acid chains in the
597 pathogenesis of autoimmune disease models. *PLoS One* **12**, e0173032 (2017).
598 47. C. Nastasi *et al.*, Butyrate and propionate inhibit antigen-specific CD8(+) T cell activation by
599 suppressing IL-12 production by antigen-presenting cells. *Sci Rep* **7**, 14516 (2017).
600 48. M. M. M. Kaisar, L. R. Pelgrom, A. J. van der Ham, M. Yazdanbakhsh, B. Everts, Butyrate Conditions
601 Human Dendritic Cells to Prime Type 1 Regulatory T Cells via both Histone Deacetylase Inhibition
602 and G Protein-Coupled Receptor 109A Signaling. *Front Immunol* **8**, 1429 (2017).
603 49. D. Ghosh, A. D. Curtis, 2nd, D. S. Wilkinson, M. D. Mannie, Depletion of CD4+ CD25+ regulatory T
604 cells confers susceptibility to experimental autoimmune encephalomyelitis (EAE) in GM-CSF-
605 deficient Csf2-/- mice. *Journal of leukocyte biology* **100**, 747-760 (2016).
606 50. T. Regen *et al.*, IL-17 controls central nervous system autoimmunity through the intestinal
607 microbiome. *Sci Immunol* **6** (2021).
608 51. A. Mangalam *et al.*, Human Gut-Derived Commensal Bacteria Suppress CNS Inflammatory and
609 Demyelinating Disease. *Cell Rep* **20**, 1269-1277 (2017).
610 52. S. K. Shahi *et al.*, Prevotella histicola, A Human Gut Commensal, Is as Potent as COPAXONE(R) in
611 an Animal Model of Multiple Sclerosis. *Front Immunol* **10**, 462 (2019).
612 53. E. Cekanaviciute *et al.*, Gut bacteria from multiple sclerosis patients modulate human T cells and
613 exacerbate symptoms in mouse models. *Proc Natl Acad Sci U S A* **114**, 10713-10718 (2017).
614 54. C. A. Lozupone, J. I. Stombaugh, J. I. Gordon, J. K. Jansson, R. Knight, Diversity, stability and
615 resilience of the human gut microbiota. *Nature* **489**, 220-230 (2012).
616 55. M. Sun *et al.*, Microbiota-derived short-chain fatty acids promote Th1 cell IL-10 production to
617 maintain intestinal homeostasis. *Nat Commun* **9**, 3555 (2018).
618 56. K. Takata *et al.*, The lactic acid bacterium Pediococcus acidilactici suppresses autoimmune
619 encephalomyelitis by inducing IL-10-producing regulatory T cells. *PLoS One* **6**, e27644 (2011).
620 57. M. Priyadarshini, K. U. Kotlo, P. K. Dudeja, B. T. Layden, Role of Short Chain Fatty Acid Receptors
621 in Intestinal Physiology and Pathophysiology. *Compr Physiol* **8**, 1091-1115 (2018).
622 58. L. Hoyles *et al.*, Microbiome-host systems interactions: protective effects of propionate upon the
623 blood-brain barrier. *Microbiome* **6**, 55 (2018).
624 59. Y. P. Silva, A. Bernardi, R. L. Frozza, The Role of Short-Chain Fatty Acids From Gut Microbiota in
625 Gut-Brain Communication. *Front Endocrinol (Lausanne)* **11**, 25 (2020).
626 60. V. Braniste *et al.*, The gut microbiota influences blood-brain barrier permeability in mice. *Sci Transl*
627 *Med* **6**, 263ra158 (2014).
628 61. A. Duscha *et al.*, Propionic Acid Shapes the Multiple Sclerosis Disease Course by an
629 Immunomodulatory Mechanism. *Cell* **180**, 1067-1080 e1016 (2020).
630 62. V. P. Kashi, S. B. Ortega, N. J. Karandikar, Neuroantigen-specific autoregulatory CD8+ T cells inhibit
631 autoimmune demyelination through modulation of dendritic cell function. *PLoS One* **9**, e105763
632 (2014).
633 63. S. Haak *et al.*, IL-17A and IL-17F do not contribute vitally to autoimmune neuro-inflammation in
634 mice. *The Journal of clinical investigation* **119**, 61-69 (2009).

64. F. Wanke *et al.*, Expression of IL-17F is associated with non-pathogenic Th17 cells. *J Mol Med (Berl)* **96**, 819-829 (2018).
65. J. L. McQualter *et al.*, Granulocyte macrophage colony-stimulating factor: a new putative therapeutic target in multiple sclerosis. *The Journal of experimental medicine* **194**, 873-882 (2001).
66. E. R. Pierson, J. M. Goverman, GM-CSF is not essential for experimental autoimmune encephalomyelitis but promotes brain-targeted disease. *JCI Insight* **2**, e92362 (2017).
67. K. Chwojnicki *et al.*, Administration of CD4(+)CD25(high)CD127(-)FoxP3(+) Regulatory T Cells for Relapsing-Remitting Multiple Sclerosis: A Phase 1 Study. *BioDrugs* **35**, 47-60 (2021).
68. S. X. Ge, D. Jung, R. Yao, ShinyGO: a graphical gene-set enrichment tool for animals and plants. *Bioinformatics* **36**, 2628-2629 (2020).

**Acknowledgments:** We thank the Waldschmidt, Legge, Jabbari, and Lieberman laboratories for helpful discussion. We thank Jian Zhang and John Harty for reading the manuscript and provinding their valuable inputs. We also thank Comparative Pathology Laboratory at the University of Iowa, Department of Pathology for their time and efforts.

**Funding:** We acknowledge funding from following sources-

National Institutes of Health/NIAID 1R01AI137075 (AKM)

Veteran Affairs Merit Award 1I01CX002212 (AKM)

University of Iowa Environmental Health Sciences Research Center, NIEHS/NIH P30 ES005605 (AKM)

Gift from P. Heppelmann and M. Wacek to (AKM)

Carver Trust Pilot Grant (AKM)

National Institute of Health training grant in Immunology T32AI007485 PI- G. Bishop (SNJ)

**Author Contributions:**

Conceptualization: AKM, SKS, NJK

Formal analysis: SKS, SG, NB, KNGC, SMG

Methodology: AKM, SKS, NB, NJK

Investigation: AKM, SKS, SNJ, SG, NB, PL, KNGC

Visualization: AKM, SKS, SNJ, SG, NB, KNGC, SMG

Funding acquisition: AKM

Project administration: AKM, SKS

Supervision: AKM, NJK

Writing – original draft: AKM, SKS, SG,

Writing – review & editing: AKM, SKS, SG, SMG, NJK

**Competing interests:** AKM is inventor of a technology claiming the use of *Prevotella histicola* for the treatment of autoimmune diseases. The patent for the technology is owned by Mayo Clinic, who has given exclusive license to Evelo Biosciences. AKM received royalties from Mayo Clinic (paid by Evelo Biosciences). However, no fund or product from the patent were used in the present study.
The remaining authors declare that the research was conducted in the absence of any commercial or financial relationships that could be construed as a potential conflict of interest.

**Data and materials availability:** All data needed to evaluate the conclusions in the manuscript are present in the manuscript and/or the Supplementary Materials. Shotgun metagenomic sequencing and RNA-seq data had been uploaded under bio-project PRJNA808406. No custom codes were used for the data analysis.

**Figures:**

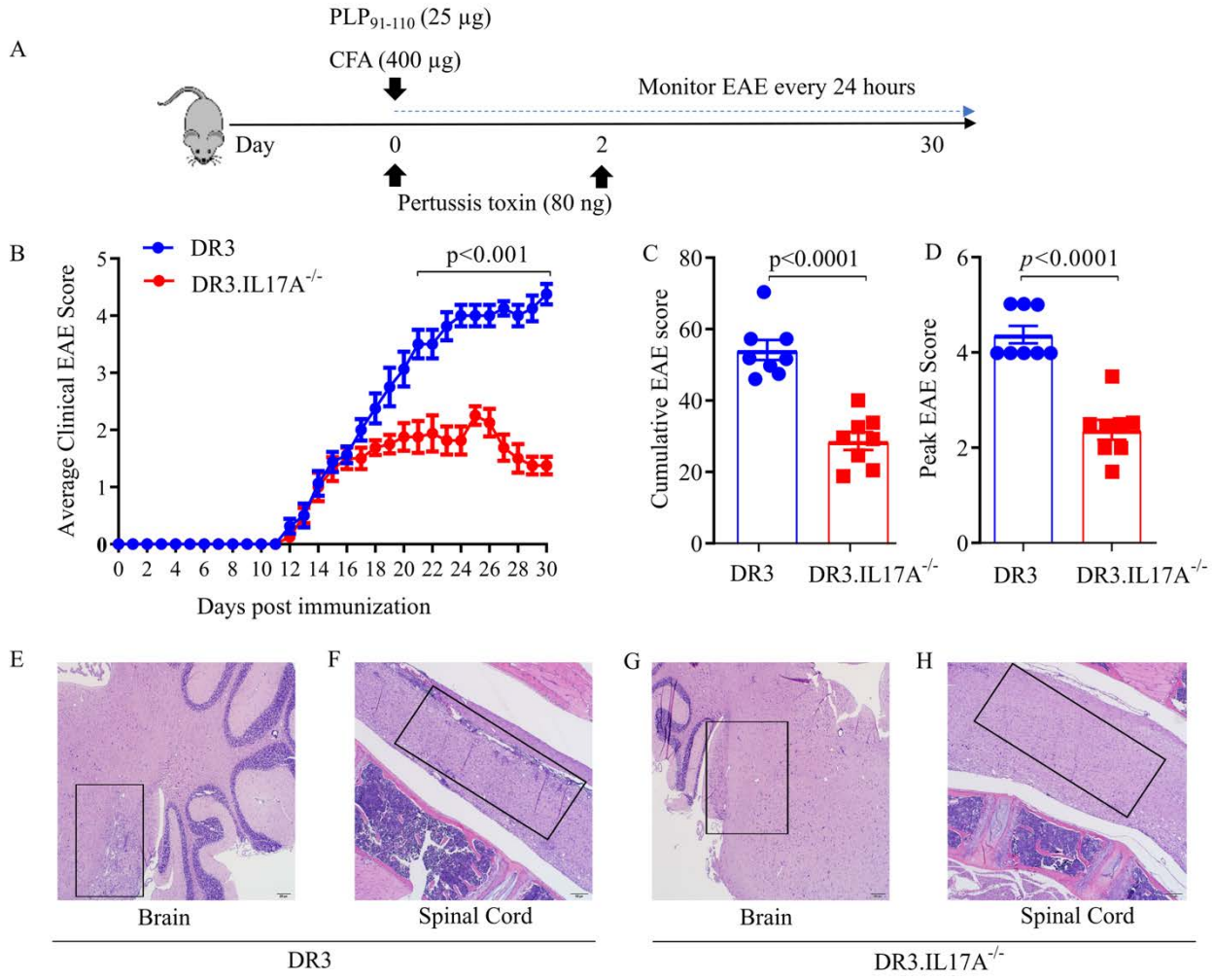


**Fig. 1: IL-17A deficiency ameliorates EAE in DR3 transgenic mice** (**A**) Schematic design of disease course in DR3 mice. HLA-DR3 (n= 8) and HLA-DR3.IL17A$^{-/-}$ (n= 8) mice were immunized with PLP$_{91-110}$ /CFA at day 0 and Pertussis toxin at days 0 and 2 to induce EAE. Mice were monitored for EAE disease progression before euthanizing on day 30 post-immunization. (**B**) Clinical EAE scores from mice in A, acquired over time. (**C**) Cumulative EAE scores from mice in A. **D**) Peak EAE score from mice in A (**E-H**) Representative histological images of tissues from the CNS from mice in A. Data are representative of 3 independent experiments with 4-5 mice per group. Bullet points (B) or bars (C, D) represent the mean and error bars represent the standard error of the mean for each experimental group. *p*-value was determined by multiple unpaired t-test (B), and unpaired t-test with Welch correction (C, D).

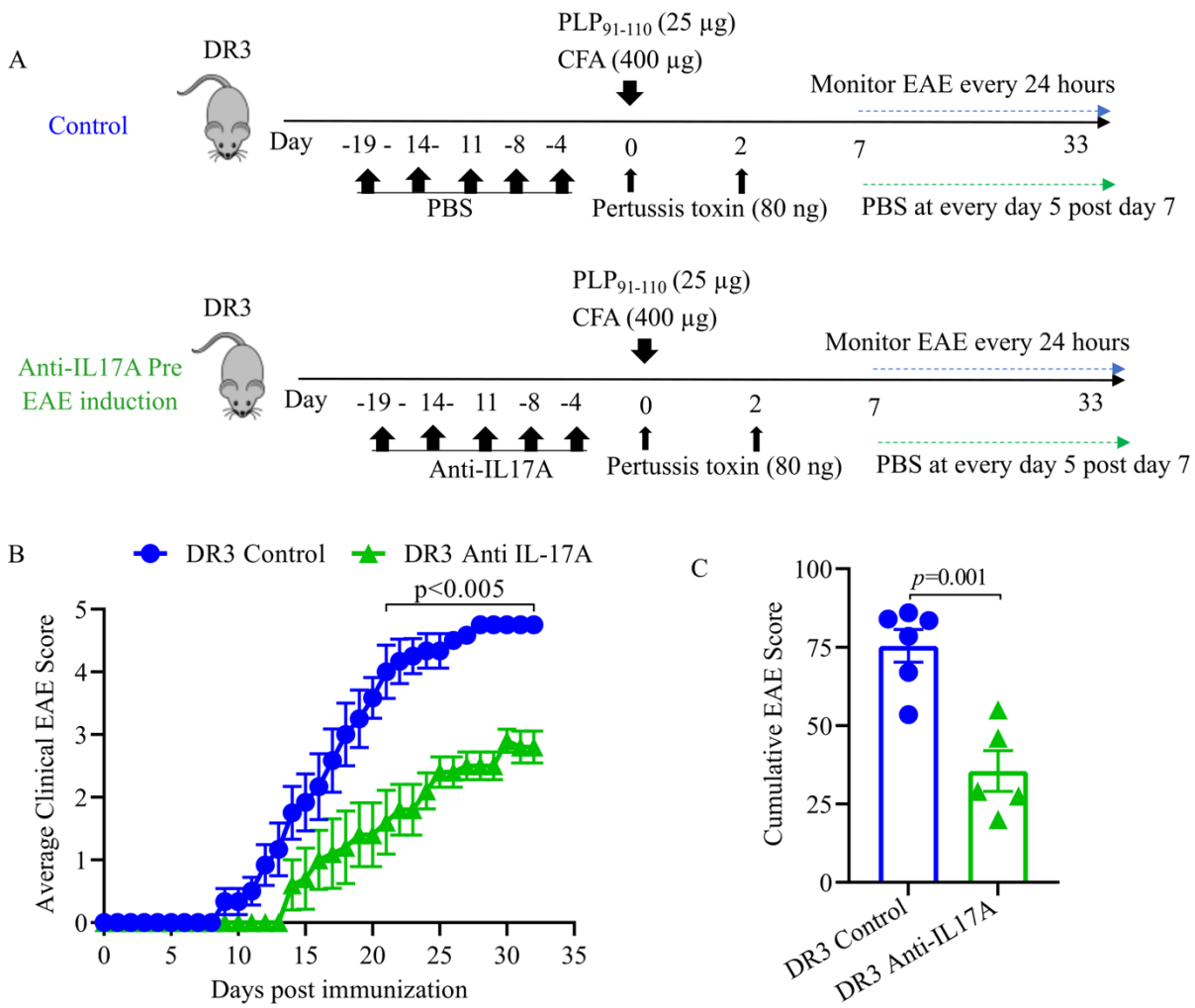


**Fig. 2: Anti-IL-17A treatment reduces the severity of EAE in HLA-DR3 mice.** (**A**) Schematic design of anti-IL-17A treatment in mice induced with EAE. 8-10-week-old HLA-DR3 mice were treated with an anti-IL-17A monoclonal antibody before EAE induction with $PLP_{91-110}$/CFA. (**B**) Average clinical EAE scores of mice treated as in A. Bullet points represent the mean and bars represent the standard error of the mean of each experimental group. (**C**) Average cumulative EAE scores of mice in A. Bars represent the mean and standard error of mean in each group. Data are from two independent experiments (n ≥4 mice per group). *p*-value determined by multiple unpaired t-test (B) and unpaired t-test with Welch correction (C).

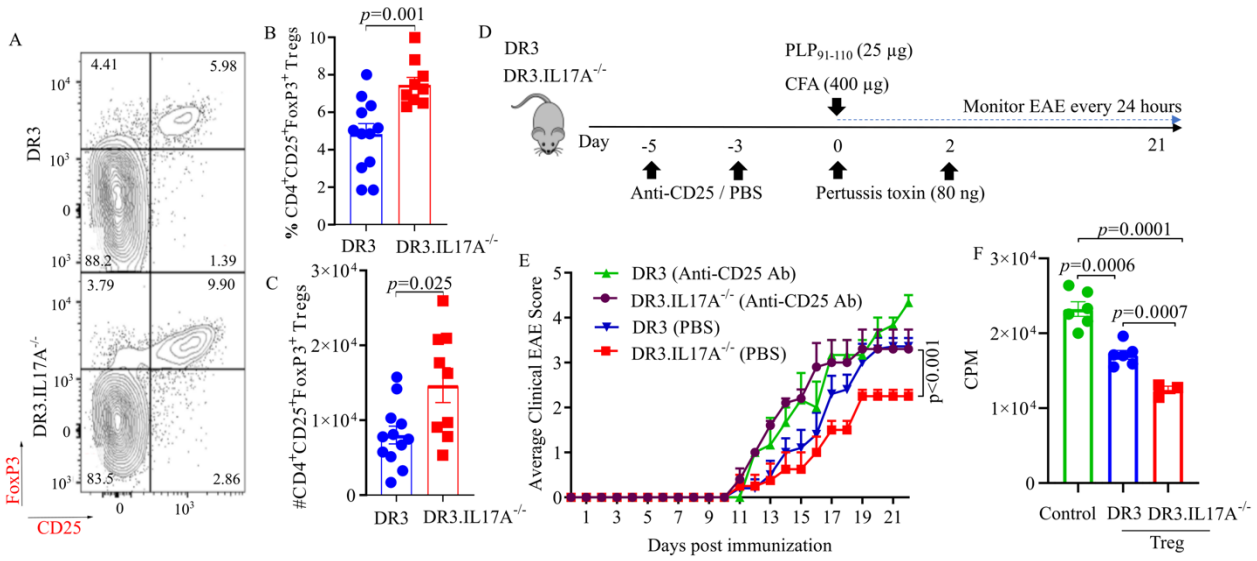


**Fig. 3: IL-17A deficiency in DR3 transgenic mice results in expansion of CD4$^+$CD25$^+$FOXP3$^+$ Treg cells.** (**A**) Representative flow cytometric plots of peripheral blood mononuclear cells (PBMCs) isolated from 8-10-week-old HLA-DR3 and HLA-DR3.IL17A$^{-/-}$ transgenic mice. Plots were gated on live lymphocytes and singlets. (B) Percentage and (C) total number of CD4$^+$CD25$^+$FoxP3$^+$ regulatory T cells from mice shown in A. (**D**) Schematic diagram of experimental workflow. HLA-DR3 and HLA-DR3.IL17A$^{-/-}$ transgenic mice were treated with anti-CD25 to neutralize Treg prior to immunization with PLP$_{91-110}$ /CFA to induce EAE. Arrowheads represent days in which mice received anti-CD25 treatment. (**E**) Average clinical EAE scores of HLA-DR3 and HLA-DR3.IL17A$^{-/-}$ mice that were treated with anti-CD25 or PBS prior to induction of EAE. (**F**) Counts per minute (CPM) of HLA-DR3 CD4 effector cells and antigen presenting cells cultured with CD4$^+$CD25$^+$ Treg from the spleen of naïve HLA-DR3 or HLA-DR3.IL17A$^{-/-}$ transgenic mice. The data represent two experiments performed at different time points. Bars represent the mean and standard error of the mean from two independent experiments. n =4-8 mice per group. *p*-value was determined by unpaired t-test with Welch correction (B, C, F) and two-way ANOVA for EAE clinical scores (E).

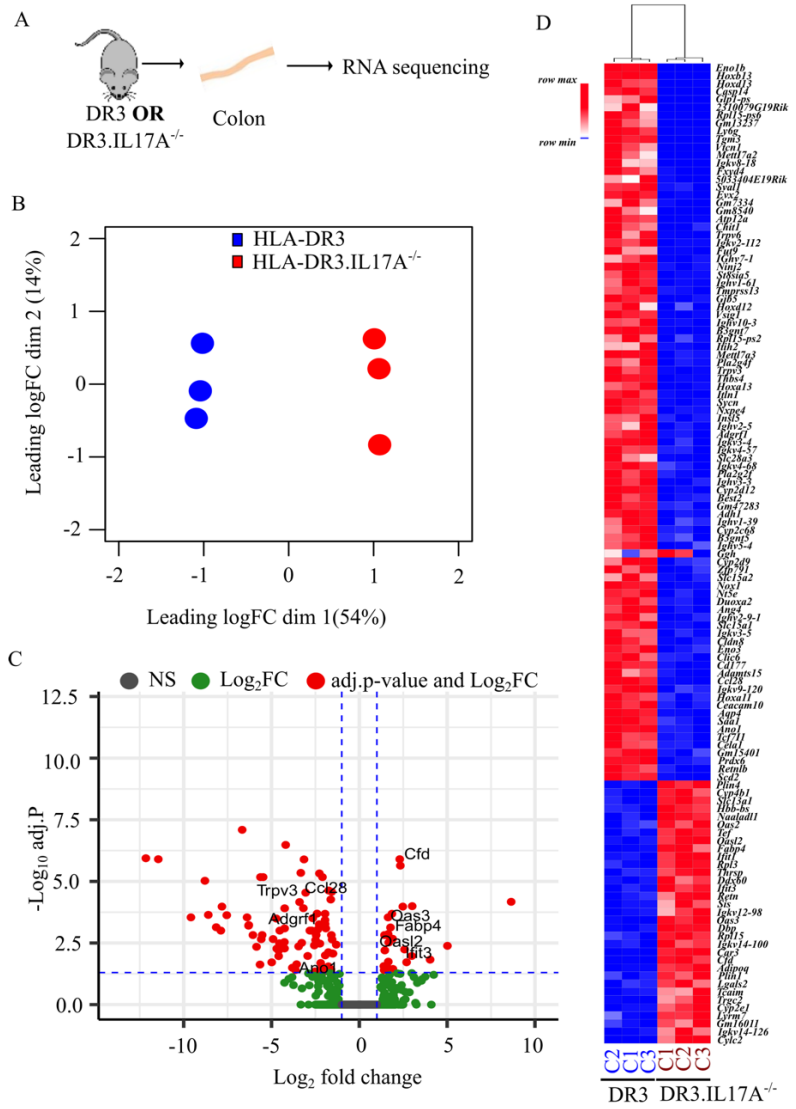


**Fig. 4: DR3 and DR3.IL17A$^{-/-}$ transgenic mice exhibit distinct gene expression patterns in the colon.** Colonic tissue was harvested from DR3 (n=3) or DR3.IL-17A$^{-/-}$ transgenic mice (n=3) and subjected to RNA-seq analysis**.** (**A**) Schematic diagram of workflow. B) Multi-dimensional scaling plot showing the separation of HLA-DR3 and HLA-DR3.IL17A$^{-/-}$ colonic samples. Each letter represents an RNA-Seq sample. Sample groups are indicated by different colors, as indicated in the legend. (**C**) Volcano plot displaying the pattern of gene expression of DR3.IL17A$^{-/-}$ mice relative to DR3 mice. Genes that are significantly differentially expressed, with a $Log_2$ fold change of >1 and an FDR-corrected p-value <0.05, are highlighted in red, blue lines represents the boundary for $Log_2$ fold change and the adjusted p-value cutoff. D) Heatmap depicting all differentially expressed genes between HLA-DR3 and HLA-DR3.IL17A$^{-/-}$ colonic samples. Labelled genes are of immunity-related categories as identified using ShinyGO webserver (68).

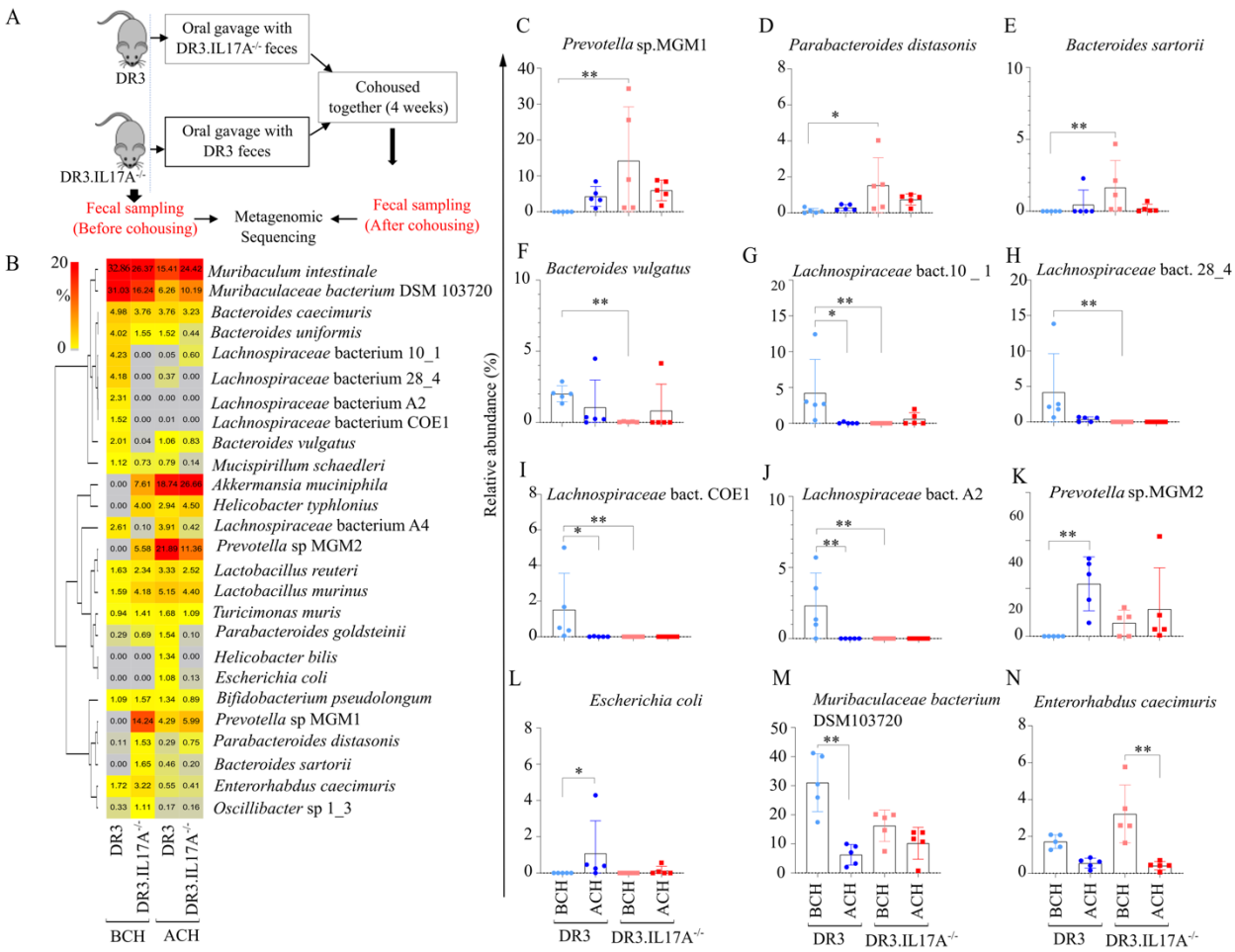


**Fig. 5: Taxonomic characterization of the gut microbiome in DR3 and DR3.IL17A$^{-/-}$ mice).** Fecal samples from DR3 and DR3.IL-17A$^{-/-}$ transgenic mice before cohousing (BCH), or after that one time fecal transferred (orally gavaged) and cohoused (ACH) were obtained and subjected to shotgun metagenomic sequencing. (**A)** Schematic diagram representing the experimental flow. B) Heatmap depicting bacterial species with > 1% average relative abundance in at least one group (n=5). (**C-N**). Statistically significantly abundant bacterial taxa that were statistically different in abundance in at least one of the comparisons (e.g., DR3-BCH to DR3IL17A$^{-/-}$-BCH, DR3-BCH to DR3-ACH, and DR3IL17A$^{-/-}$-BCH to DR3IL17A$^{-/-}$-ACH). Kruskal Wallis test followed by Dunn's *posthoc* analysis was performed to identify significant differences between groups. "*" and "**" represent significance at $p<0.05$ and $p<0.01$ respectively.

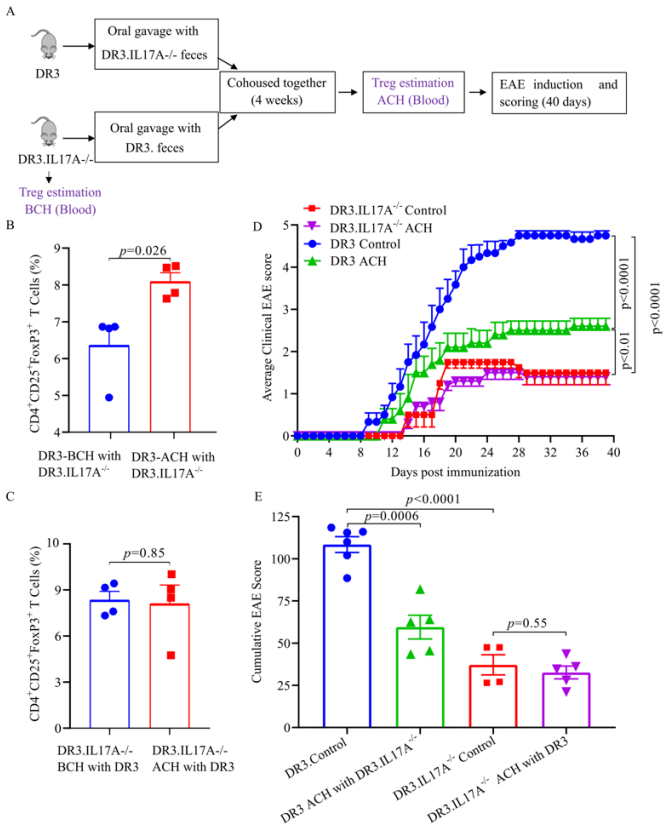


**Fig. 6: Treg-inducing bacteria from DR3.IL17A$^{-/-}$ mice reduce disease severity when transferred to DR3 mice. (A)** Schematic of experimental design showing experimental outline. 8-10-week-old female DR3 transgenic mice were cohoused for four weeks with DR3.IL17A$^{-/-}$ transgenic mice after one-time fecal transferred (orally gavaged) from each other mice strains. Peripheral blood mononuclear cells (PBMCs) were isolated from blood that was collected by retro-orbital bleeding, and regulatory T cells were assessed by flow cytometric analysis. Percentages of CD4$^{+}$CD25$^{+}$FoxP3$^{+}$ T cell populations in (**B**) DR3 transgenic mice before (BCH) and after (ACH) being cohoused with DR3.IL17A$^{-/-}$ transgenic mice and in (**C**) DR3.IL17A$^{-/-}$ transgenic mice before (BCH) and after (ACH) being cohoused with DR3 transgenic mice. (**D**) Average clinical EAE scores of DR3 transgenic mice (non-cohoused control and after cohoused with DR3.IL17A$^{-/-}$ transgenic mice) and DR3.IL17A$^{-/-}$ transgenic mice (non-cohoused control and after cohoused with DR3 transgenic mice) that were immunized with PLP$_{91-110}$/CFA and followed for 30 days. (**E**) Average cumulative EAE scores of mice in C. Data represent the mean and standard error of the mean for each experimental group from two independent experiments: n ≥4 mice per group. *p*-value was determined by unpaired t-test with Welch correction (A, B, D), two-way ANOVA for clinical EAE scores (C).

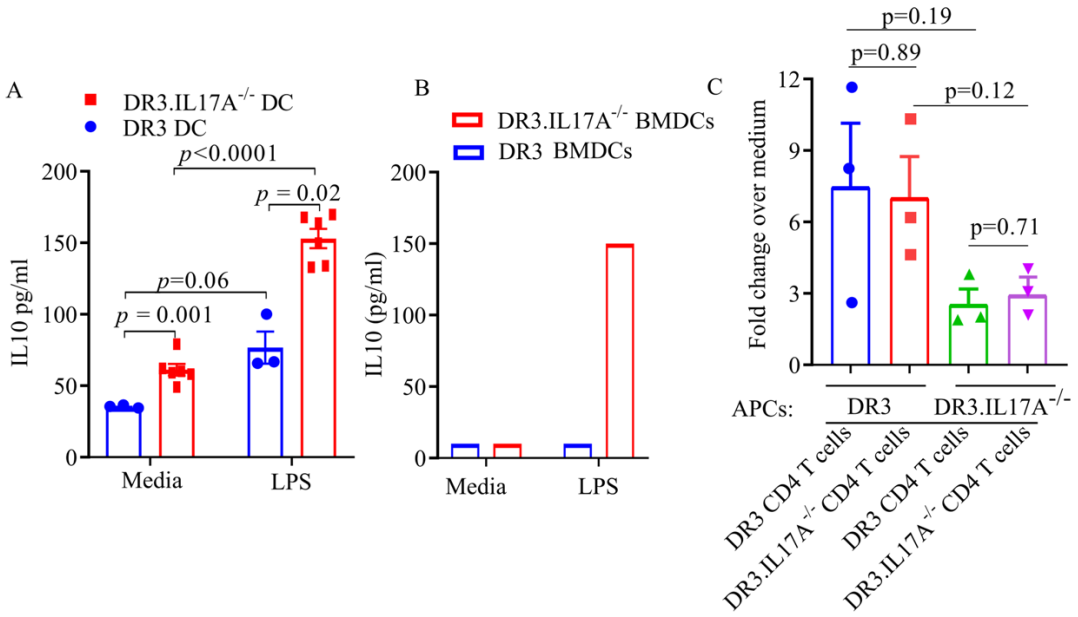


**Fig. 7**: **Dendritic cells adopt a tolerogenic phenotype in the absence of IL-17A**. (**A**) Quantification of IL-10 cytokine production in naïve dendritic cells from DR3 and DR3.IL17A$^{-/-}$ transgenic mice following stimulation with LPS. Splenocytes were harvested from naïve 8-10-week-old DR3 and DR3.IL17A$^{-/-}$ transgenic mice and CD11c+ dendritic cells were isolated using BD™ IMag Particles. Purified CD11c+ cells were activated with LPS for 24 hours and IL-10 was measured by ELISA. Media without LPS was used as control. Bars represent the mean and standard error of the mean from each experimental group; n ≥3 mice per group. p-value was determined by Mann-Whitney test. (**B**) Quantification of IL-10 cytokine production from bone marrow-derived DCs (BMDCs). Bone marrow was collected from naïve DR3 or DR3.IL17A$^{-/-}$ transgenic mice and cultured in the presence of GM-CSF and IL4 for 4 days. BMDCs were then cultured with or without LPS for 24 hours and IL-10 was measured by ELISA. (**C**) Antigen-specific proliferation of CD4+ T cells from DR3 and DR3.IL17A$^{-/-}$ transgenic mice. 8-10-week-old DR3 and DR3.IL17A$^{-/-}$ transgenic mice were immunized with PLP$_{91-110}$/CFA. After 7 days, mice were euthanized, and splenocytes were harvested to isolate CD4$^{+}$ T cells using BD™ IMag Particles. CD4+ T cells and antigen presenting cells were cultured together in presence of PLP$_{91-110}$ for 5 days, and thymidine was added in the last 12 hours of culture. CD4$^{+}$ T cells from mice of either genotype were cultured in the presence of antigen presenting cells. Bars represent the mean and standard error of the mean from each experimental group after subtracting the baseline medium values. n =3 mice in each group; *p*-value determined by unpaired t-test with Welch correction (A, C).

# Supplementary Materials

## Materials and methods

### Study design

The study utilized female HLA-DR3 and HLA-DR3.IL17A$^{-/-}$ transgenic mice to investigate the contributions of IL-17A to EAE. Disease was induced by immunizing mice with the PLP$_{91-110}$ peptide. The number of sample sizes are indicated in the figure captions. The disease induction and scoring of the EAE was performed as described below and elsewhere (*1*). No data, including outliers, were excluded from the analysis. Experiments were performed at least twice with some exceptions as indicated in the figure legends.

### Mouse procurement, disease induction, and scoring

HLA-DR3 (DRA1*0101, DRB1*0301) transgenic mice on the B6/129 background have been characterized previously (Das et al., 2000; Mangalam et al., 2009). These mice lack endogenous murine major histocompatibility complex (MHC) class II genes (AE$^{-/-}$) and express alleles DRA1*0101, DRB1*0301, as described previously (Das et al., 2000; Mangalam et al., 2009). The HLA-DR3.IL17A$^{-/-}$ mice (referred to as DR3.IL17A$^{-/-}$) that were used in this study were generated by crossing HLA-DR3 (referred to as DR3) and AE$^{-/-}$.IL17A$^{-/-}$ mice and validated using genotyping. C57BL/6 mice were also utilized in this study and were purchased from the Jackson Laboratories (Bar Harbor, ME). Female mice DR3.IL17A$^{-/-}$ and C57BL/6 mice (8-10 weeks of age) were used in this study. Mice were bred and maintained in the University of Iowa animal facility in accordance with NIH and institutional guidelines. All experiments were approved by the Institutional Animal Care and Use Committee at the University of Iowa.

To induce EAE in mice, DR3 and DR3.IL17A$^{-/-}$ transgenic mice (8 to 12 weeks old) were immunized subcutaneously in both flanks with 50 µg of PLP$_{91–110}$ (YTTGAVRQIFG DYKTTICGK) (GenScript, Piscataway NJ, USA) that was emulsified in CFA containing 200 µg/mouse *Mycobacterium tuberculosis* H37Ra (Becton, Dickinson and Company, Sparks, MD, USA). 80 ng of pertussis toxin (PTX) (Sigma Chemicals, St. Louis, MO; 100 ng) was given intraperitoneal at day 0 and 2 post immunization. C57BL/6 mice were immunized subcutaneously in both flanks with MOG$_{35-55}$ CFA/PTX, as just described for immunization with PLP (*2*). Mice

were observed daily for disease symptoms and EAE was scored with the following scoring system, as described previously (*1*): normal, 0; loss of tail tone, 1; hind limb weakness, 2; hind limb paralysis, 3; hind limb paralysis and forelimb paralysis or weakness, 4; and morbidity/death, 5.

**Pathology**

Brains and spinal cords were collected from DR3, and DR3.IL17A$^{-/-}$ transgenic mice at day 30 post immunization. Histological analysis was performed to assess inflammation and demyelination, as described previously (*3, 4*). Briefly, DR3 and DR3.IL17A$^{-/-}$ transgenic mice were perfused with approximately 50 ml of 10% neutral buffered formalin via intracardiac puncture. The calvaria and spinal columns were collected, and immersion fixed in 10 % neutral buffered formalin (10% BFA) for 24-48 hours followed by decalcification in EDTA for approximately 24 hours. Decalcified tissues were cut into 2 mm coronal blocks, embedded in paraffin and routinely processed. The slide were cut at 4-5 mm thickness and stained with hematoxylin and eosin. HE-stained slides including the brainstem, cortex, corpus callosum, cerebellum, hippocampus, and striatum were examined and scored by a board-certified veterinary pathologist as described previously (*3, 4*).

**Flow cytometry**

Peripheral blood mononuclear cells (PBMCs) were isolated from naïve DR3 and DR3.IL17A$^{-/-}$ transgenic mice using Histopaque-1077 (Millipore Sigma, USA) density centrifugation method as per instructions from the manufacturer (Sigma-Aldrich, St. Louis, USA). Briefly, 200 µl of blood was collected in an EDTA-containing Eppendorf tube by retroorbital bleeding. Blood was diluted with 800 ml of phosphate-buffered saline (PBS; Gibco/Lubioscience) and added to 1 ml of Histopaque-1077, and then centrifuged at 400 x g for 30 minutes at room temperature, without the brake. Following centrifugation, the buffy coat was collected into 5 mL tubes and washed with PBS (400 x g for 10 minutes at 4°C). The cells were washed with FACS buffer stained with antibodies to detect surface expression of CD4 (GK1.5) and CD25 (PC61) (BD Biosciences, Franklin Lakes, NJ), whereas intracellular expression of FoxP3$^{+}$ was stained using an anti-Mouse/Rat FoxP3 (FJK-16s) staining kit (eBiosciences, San Diego, CA). Intracellular staining for IL17, IFNγ, and GM-CSF were performed using the intracellular fixation permeabilization kit and anti-mouse IL17 (TC11-18H10.1), IFNγ (XMG1.2), and GM-CSF (MP1-22E9) specific

antibodies from eBioscience™. Cells were also stained with antibodies to detect surface expression of CD45 (30-F11) and CD4 (clone GK1.5) to gate on the leukocyte population.

**T cell proliferation and cytokine assay**

Mice were euthanized 10 days after immunization with $PLP_{91–110}$ and draining lymph nodes were removed and challenged *in vitro* with $PLP_{91–110,}$ as described previously (Mangalam et al., 2004 Eur. J. Immunol. 34: 280–290). The results are presented as stimulation indices, which are counts per minute (cpm) of test sample/cpm of the control). For cytokine analysis, supernatants were collected from culture 48 h after peptide stimulation, and the concentration of cytokines (IL-17F, and GM-CSF) were measured by sandwich ELISA using pairs of relevant anti-cytokine monoclonal antibodies (Pharmingen, San Diego, CA).

**Isolation of $CD4^+CD25^+$ Treg, $CD4^+CD25^-$ T effector, and Dendritic cells**

$CD4^+CD25^+$ T cells isolated from the spleens of DR3 and DR3.IL17A$^{-/-}$ transgenic mice using the EasySep™ Mouse $CD4^+CD25^+$ regulatory T Cell Isolation Kit II (STEMCELL Technologies, Vancouver, Canada) according to the manufacturer's protocols. $CD4^+CD25^-$ T effector cells were isolated from the Treg-depleted fraction of splenocytes using Anti-Mouse CD4 Magnetic Particles – DM (BD Biosciences, CA, USA). DCs were isolated from total splenocytes using CD11c microbeads according to the manufacturer's protocols (BD Biosciences, CA, USA). The purity of specific cell populations was analyzed by flow cytometry; all populations used were >90% pure.

***In vivo* depletion of $CD4^+CD25^+$ Treg cells**

DR3 and DR3.IL17A$^{-/-}$ transgenic mice received two intraperitoneal injections (200 µg/injection) of monoclonal anti-mouse CD25 (IL-2Ra) antibody (clone: PC-61.5.3; BioXcell) in 200 µl of PBS per dose on days -5 and -3 before induction of EAE (5). Controls received two intraperitoneal injections of 200 µl of PBS. $CD4^+CD25^+FoxP3^+$ T cell depletion was confirmed by flow cytometric analysis of PBMCs on the day EAE was induced. For IL-17A depletion, DR3 transgenic mice were injected intraperitoneally with 100 ug/mouse anti-IL17A (Clone 17F3; BioXcell), IgG1 (Clone MOPC-21; BioXcell) or PBS. IL-17A was blocked in C57BL/6 mice by administering 100 ug/mouse anti-IL-17A, IgG1 or PBS by intraperitoneally injection every three days following induction of EAE, starting at day 5 through day 32 (e.g., days -24, -21, -18, -15, -

12, -9, -6 and -3 pre EAE induction and post EAE induction (at day 5, 8, 11, 14, and 17). IL-17F or GM-CSF cytokine inhibition was performed *in vivo* in DR3.IL17A$^{-/-}$ transgenic mice by intraperitoneally injection of 100µg/mouse anti-IL-17F (clone; MM17F-8F5; BioXcell) or 100µg/mouse of anti-GM-CSF (clone; MP1-22E9; BioXcell) post induction of EAE on days 5, 10, and 14. Control DR3.IL17A$^{-/-}$ transgenic mice received 100µg/mouse IgG1 (Clone MOPC-21; BioXcell).

**Treg suppression assay**

Spleens from 8-10-week-old DR3 and DR3.IL17A$^{-/-}$ transgenic mice were harvested for CD4$^{+}$ T cells by BD™ IMag Particles as per manufacturer instruction. T cell-depleted splenocytes were used as antigen presenting cells after UV irradiation. CD4$^{+}$CD25$^{+}$ T cells were isolated from splenocytes of DR3 and DR3.IL17A$^{-/-}$ transgenic mice using EasySep™ Mouse CD4$^{+}$CD25$^{+}$ regulatory T cell isolation kit II (STEMCELL Technologies, Vancouver, Canada) according to the manufacturer's protocols. Treg suppression assays were performed as described previously (*6*).

**Co-housing of DR3 and DR3.IL17A$^{-/-}$ transgenic mice**

For fecal transplantation, DR3.IL17A$^{-/-}$ transgenic mice were recipients of fecal transplants from DR3 transgenic mice through oral gavage, and conversely, DR3 transgenic mice were recipients of fecal transplants from DR3.IL17A$^{-/-}$ transgenic mice through oral gavage. Five days after oral gavage, DR3 transgenic mice were cohoused with DR3.IL17A$^{-/-}$ transgenic mice. Fecal samples were collected before and after co-housing for shotgun metagenomic sequencing.

**Microbiota DNA isolation, sequencing, and analysis**

Five female mice of each genotype, DR3 and DR3.IL17A$^{-/-}$, were assessed for the composition of their gut microbiota before and after cohousing, resulting in a total of 20 fecal samples. DNA was extracted using PowerSoil DNA Isolation Kit (Qiagen) following the manufacturer's protocol. Each metagenomic DNA was quantified and sequenced using an Illumina MiSeq resulting in more than 55 Gb of raw paired-end reads from 20 samples after shotgun metagenomic sequencing. The raw paired-end metagenomes were quality trimmed using Trim Galore version 0.5.0 (*7*), followed by host read filtering by mapping to the mouse genome (GRCm39) using Bowtie2 (*8*), with default parameters resulting in 49.43 Gb of high-quality data. The quality trimmed and filtered forward

and reverse reads were taxonomically characterized using MetaPhlAN 3.0 (*9*) and mpa_v30_CHOCOPhlAN_201901 database with default parameter settings. The obtained relative percentages of the microbial taxa were compared between the groups using Kruskal-Wallis test followed by Dunn's multiple t-test in GraphPad Prism unless stated otherwise. The filtered and trimmed sequences were further assembled using MegaHit (*10*). After assembly, Prokka was used to predict ORF based protein coding genes and assign functions to the predicted genes (Seemann T, 2014). BBMap aligner was used to produce quantifiable gene counts in the FPKM format (fragments per kilobase of gene per million) (https://jgi.doe.gov/data-and- tools/bbtools/). InterProScan was utilized for assignment for KEGG pathways and GO processes (https://www.ebi.ac.uk/interpro/search/sequence/). FPKM values of every protein/gene assigned to each of the KEGG pathway or GO process were derived from mapping the gene to the FPKM list of the genes identified in the previous step. Relative abundances of genes and pathways were used for the downstream statistical analysis. Statistical significance between the groups were determined using non-parametric Wilcoxon signed rank test, and data visualized using GraphPad Prism.

**In vivo depletion of IL-17A in C57BL/6 mice**

C57BL/6 mice were placed in three groups that received antibody injections prior to EAE induction (day -24, -21, -18, -15, -12, -9, -6, and -3): the first group of mice received intraperitoneal injections (200 µg/injection) of monoclonal anti-mouse IL-17A (clone 17F3; BioXCell) in 200µl PBS per dose; the second group of mice received 200 µg/injection of isotype control (mouse IgG1) in 200µl PBS per dose; and the third group of mice received 200µl PBS to serve as vehicle control. Similarly, three groups of C57BL/6 mice were treated with either monoclonal anti-mouse IL-17A (200 µg/injection), isotype control mouse IgG1 (200 µg/injection), or PBS starting on day 5 post EAE induction, and continuing every third day until day 32. Mice were observed daily for disease symptoms and EAE was scored as per the scoring system described (*11*).

**Transcriptome sequencing and analysis**

Tissue sections from the colon of both DR3.IL17A$^{-/-}$ and DR3 mice before EAE induction were collected, chopped into small pieces, stored in RNAlater (Millipore Sigma, MO, USA), and frozen to -80$^{0}$C until further use. RNA was extracted using the RNeasy Kit (Qiagen) following the

manufacturer's instructions. The quality and quantity of the RNA was evaluated using a NanoDrop and sequenced at Novogene Co. Ltd, CA. Sequences were quality controlled using default *fastqc* (*12*). Paired FASTQ files were aligned to the mm10 genome build with the kallisto pseudoaligner (*13*) using 100 bootstraps. Estimated counts for transcripts were then aggregated into gene-level quantifications based on gene symbol. An average of 14.79 ±1.3 million transcripts were obtained for each sample. Further downstream processess were then carried out in R 4.0.3 (*14*) using edgeR 3.32.1 (*15*) to identify differentially expressed genes, as described previously. Differentially expressed genes were fed into ShinyGO (*16*) to identify changes to genes involved in GO biological pathways using the mouse reference database.

## Supplementary Figures

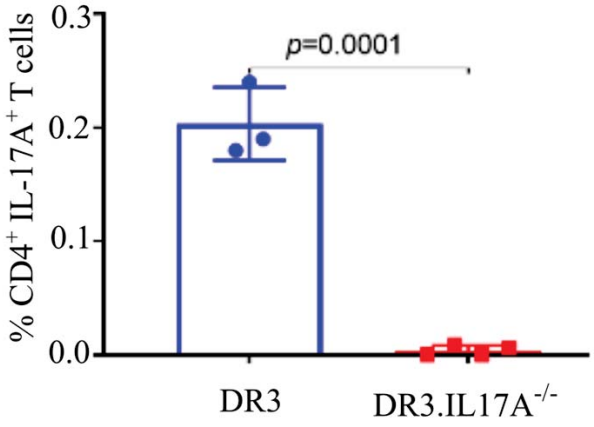


**Fig. S1: HLA-DR3.IL17A$^{-/-}$ mice lack IL-17A-expressing CD4+ T cells in the spleen.** 8-10-week-old HLA-DR3 and HLA-DR3.IL17A$^{-/-}$ transgenic mice were euthanized and splenocytes were harvested for analysis. Quantification of the frequency of CD4$^{+}$IL-17A$^{+}$ T cells from mice in A. HLA-DR3: n=3; HLA-DR3.IL17A$^{-/-}$: n = 4. *p*-value was determined using Mann-Whitney test between the experimental groups. Symbols represent individual mice, bars represent mean±SEM.

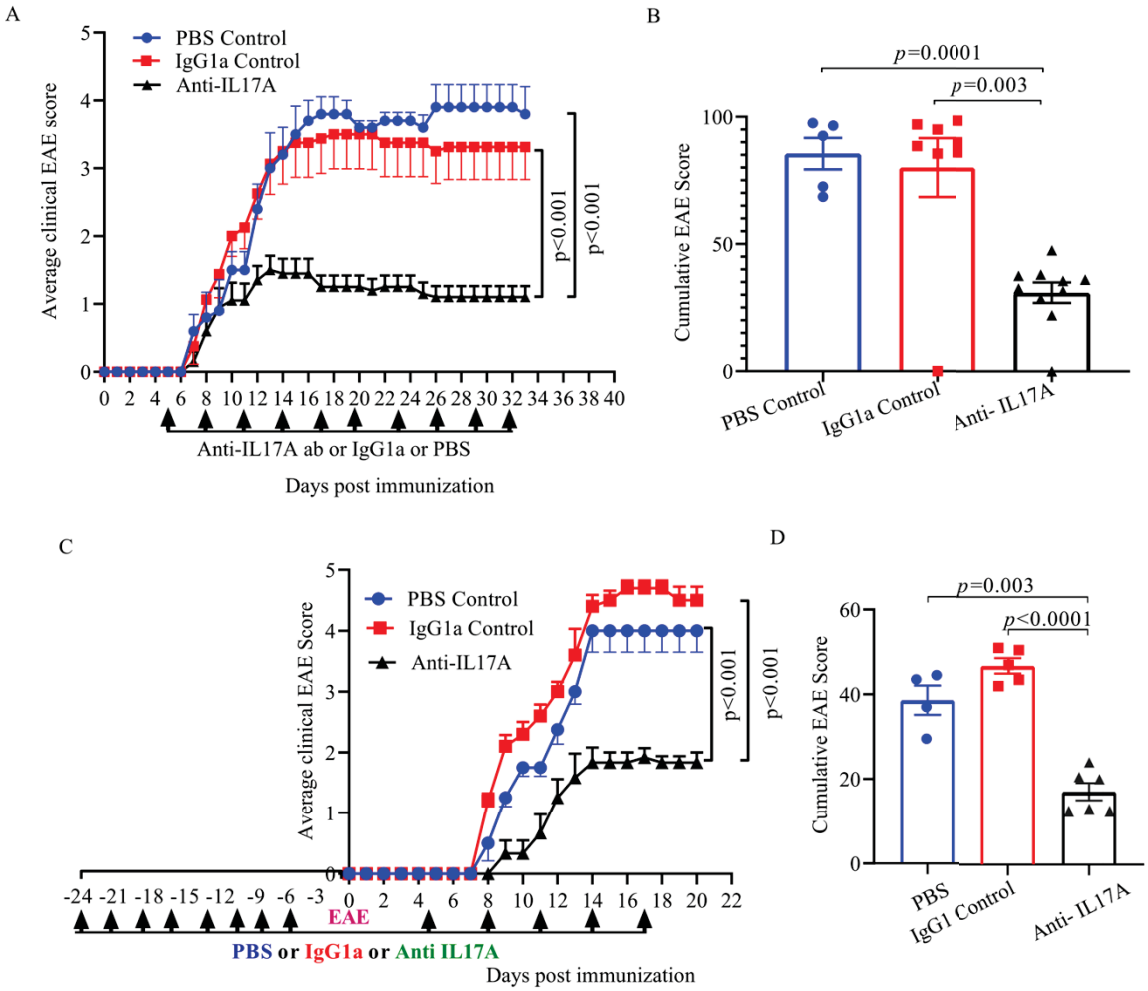


**Fig. S2: Anti-IL-17A treatment lowers the severity of $MOG_{35-55}$ induced EAE in C57BL/6J mice. (A-B)** 8-10-week-old B6 mice were immunized with $MOG_{35-55}$/CFA. Five days after immunization, mice received anti-mouse IL-17A monoclonal antibody, isotype control mouse IgG1, or PBS intraperitoneally every three days until the end of the experiment (day 32). (A) Average clinical EAE scores over time. Treatment days are indicated by arrowheads. (B) Average cumulative EAE scores. (**C-D**) 8-10-week-old B6 mice were treated every three days with anti-IL-17A, IgG1, or PBS pre- and post-immunization with $MOG_{35-55}$/CFA. (C) Average clinical EAE scores. Treatment days are indicated by arrowheads. (D) Average cumulative EAE scores. For plots in A, C, each bullet point represents the mean and bars represent the standard error of the mean from each experimental group. *p*-value was determined using two-way ANOVA following Tukey correction for EAE clinical scores (A, C) and unpaired t-test with Welch correction for cumulative EAE score (B, D). For graphs in B, D, each bar represents mean±SEM.

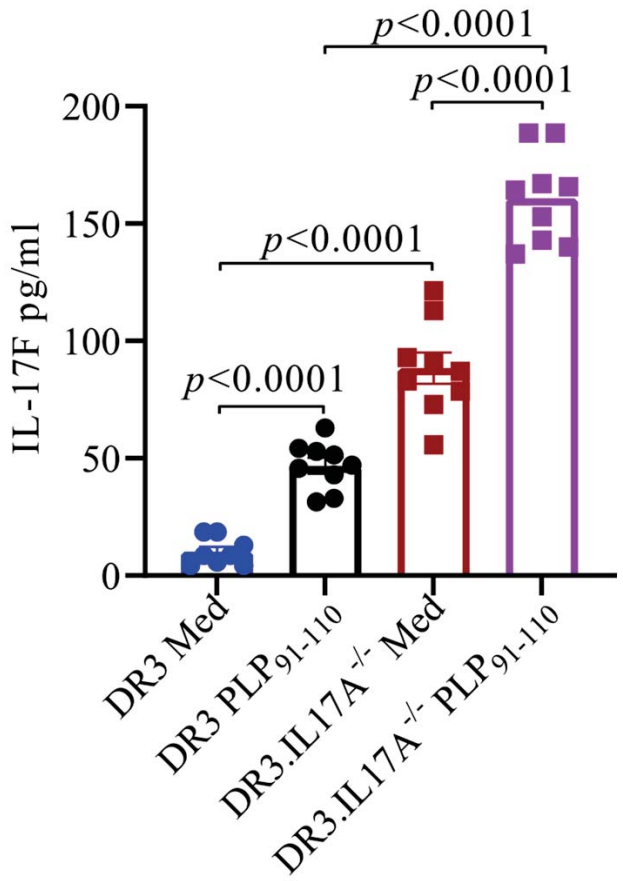


**Fig. S3: Levels of inflammatory cytokines IL-17F in HLA-DR3 and HLA-DR3.IL17A$^{-/-}$ mice.** 8-10-week-old mice were immunized with $PLP_{91-110}$ /CFA to induce EAE. After 20 days, mice were euthanized, spleens were harvested, and splenic cells were cultured in the presence of $PLP_{91-110}$ antigen for five days following stimulation with Phorbol myristate acetate (PMA) and ionomycin in the presence of Brefeldin A (BFA). The supernatant was collected and levels of IL17F were measured using ELISA. Cytokine values from DR3 mice were compared to those of DR3.IL17A$^{-/-}$ mice in either media (Med) or after stimulation with $PLP_{91-110}$. *p*-value was determined using unpaired t-test with Welch correction. Bars represent mean±S.E.M.

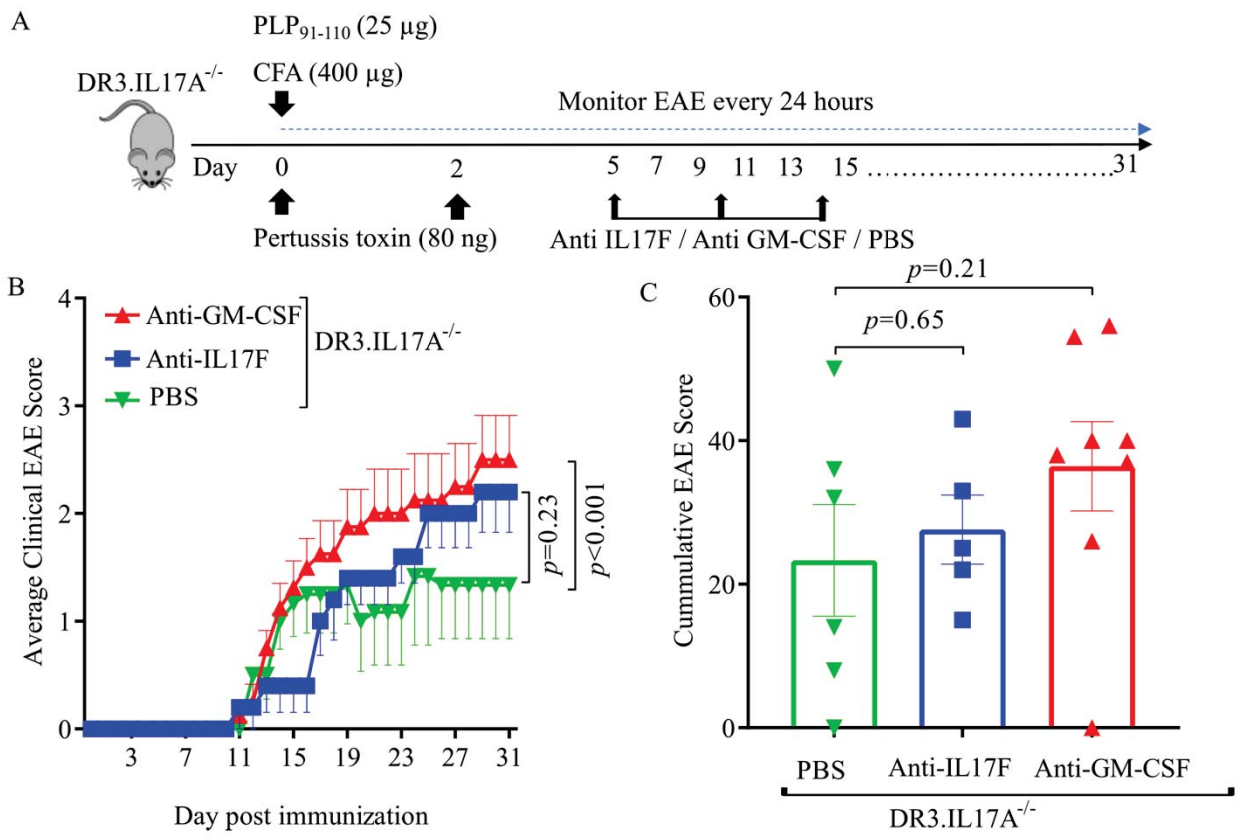


**Fig. S4: Treatment with anti-GM-CSF or anti-IL-17F monoclonal antibodies increases disease severity in HLA-DR3.IL17A$^{-/-}$ mice.** (**A**) Schematic diagram of the experimental workflow. EAE was induced in 8-10-week-old in HLA-DR3.IL17A$^{-/-}$ transgenic mice. At days 5, 10, and 14 post-EAE induction, mice received intraperitoneal injections of either: 1) anti-GM-CSF monoclonal antibody, 2) anti-IL-17F monoclonal antibody, or 3) IgGa1 isotype control and clinical EAE scores were monitored for 31 days. (**B**) Average clinical EAE score of mice in each group over time. Bullet points represent the mean and bars represent the standard error of the mean of each experimental group from two independent experiments (n ≥3 mice per group). *p*-value was determined by a two-way ANOVA following Tukey correction for average clinical EAE score (B). (**C**) Average cumulative EAE scores. *p*-value was determined by unpaired t-test with Welch correction (C). For plots in B, C, each symbol represents the mean and bars represent the standard error of the mean from each experimental group.

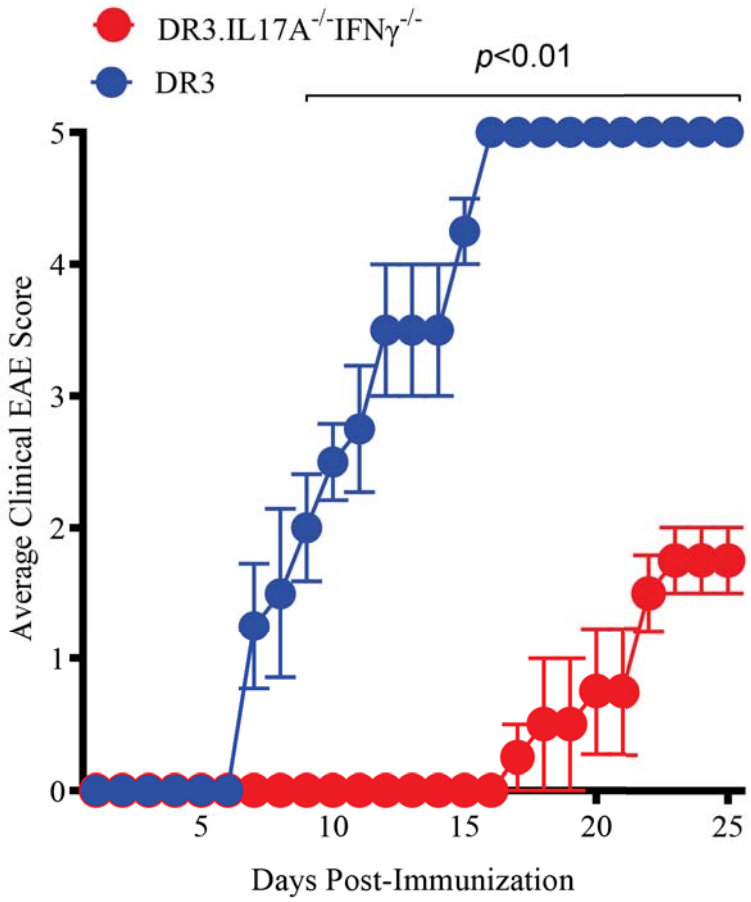


**Fig. S5: HLA-DR3.IL17A$^{-/-}$ mice develops milder EAE in absence of IFNγ .** EAE was induced in 8-10-week-old in HLA-DR3 and HLA-DR3.IL17A$^{-/-}$IFNγ$^{-/-}$ transgenic mice using $PLP_{91-110}$, CFA and PTX. The disease was monitored and scored daily until day 25 of the experiment. Average clinical EAE score of mice in each group over time. Bullet points represent the mean and bars represent the standard error of the mean of each experimental group from two independent experiments (n =4 mice per group). *p*-value was determined by multiple unpaired t-tests with correction using two-stage step up method of Benjamini, Krieger and Yekutieli for average clinical EAE score.

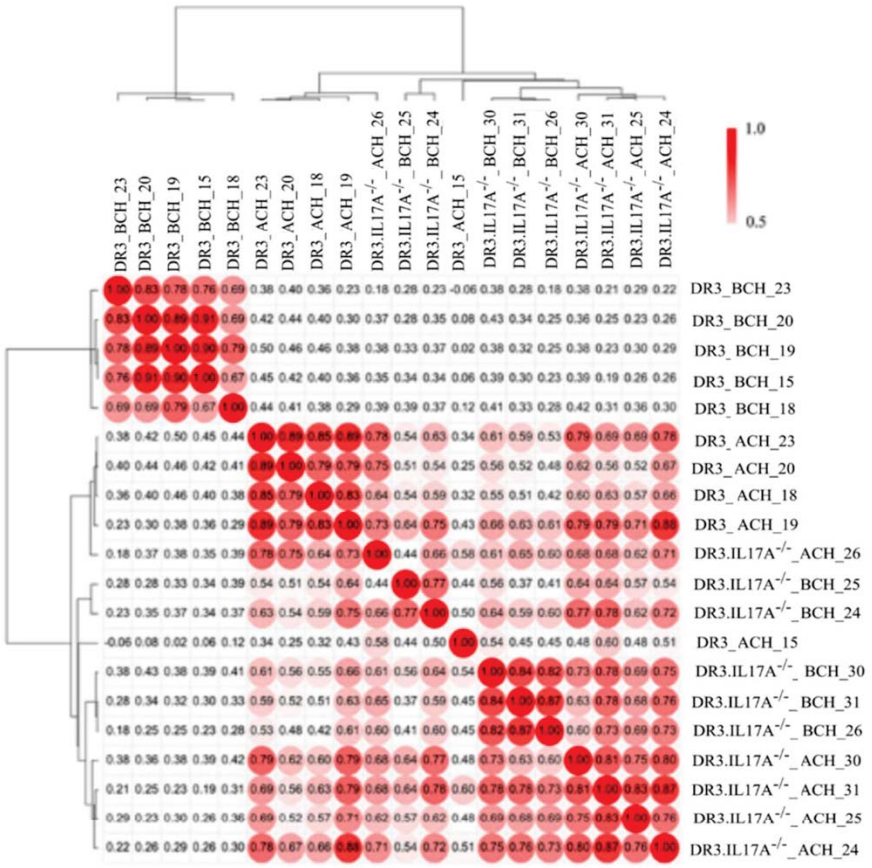


**Fig. S6:** Similarity matrix of microbial compositional communities present in DR3 and DR3.IL17A$^{-/-}$ mice before (BCH) and after (ACH) cohousing. Matrix was computed from the relative abundance matrix using 1-Spearman rank correlation metric using average linkage method and clustered hierarchically using Morpheus webserver (https://software.broadinstitute.org/morpheus).

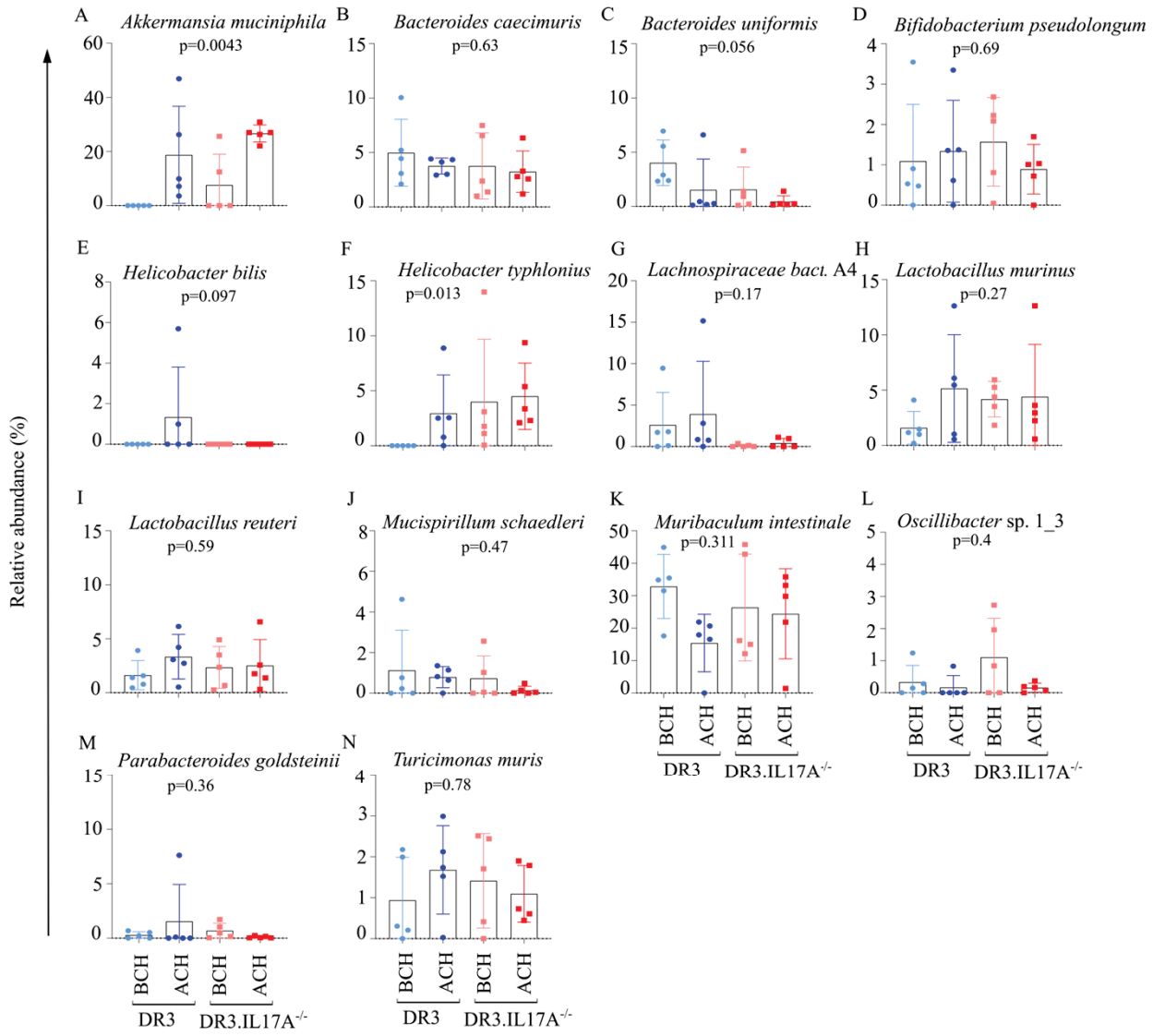


**Fig. S7:** Composition of the gut bacteria in DR3 and DR3IL17A$^{-/-}$ transgenic mice before (BCH) and after (ACH) mice were cohoused. Each bar represents the average relative abundance (%) of the bacterium in each group. Kruskal Wallis test followed by Dunn-test was performed to identify the significance between the groups. 'p-value' from A-N represents the significance for the Kruskal Wallis test. Those bacteria with significant/non-significant p-value from Kruskal Wallis test but non-significantly different in at least one of the groups of interest (DR3-BCH to DR3IL17A$^{-/-}$-BCH, DR3-BCH to DR3-ACH and DR3IL17A$^{-/-}$-BCH to DR3IL17A$^{-/-}$-ACH) following Dunn test are shown.

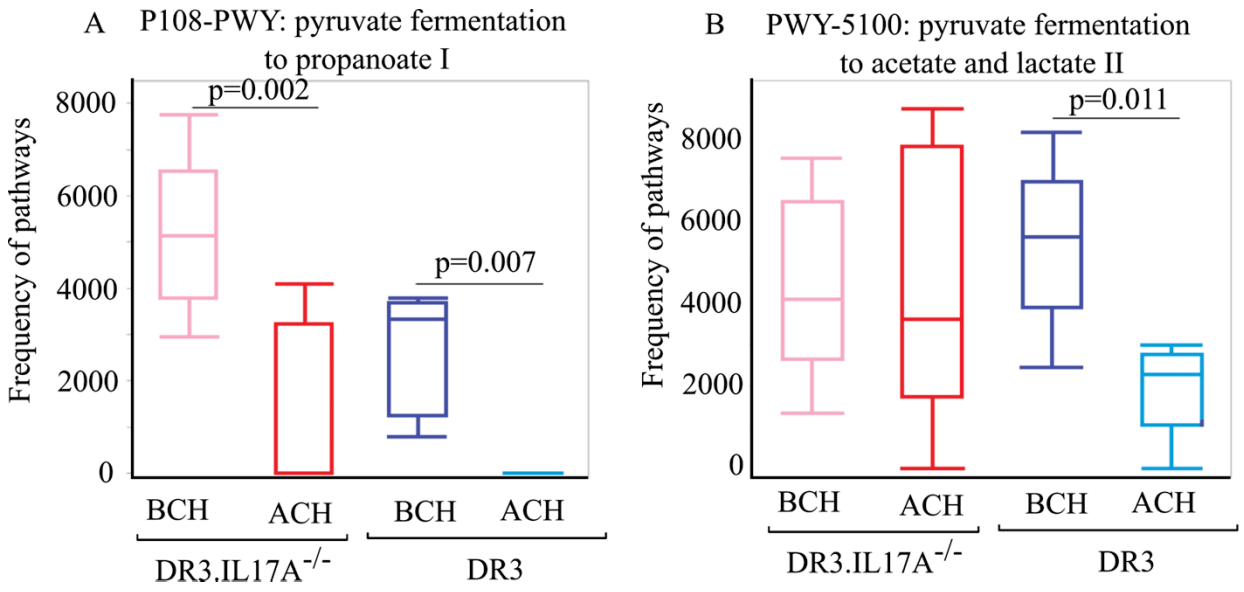


**Fig. S8**: Abundance of short chain fatty acid pathways, as determined by shotgun metagenomics analysis in DR3.IL17$^{-/-}$ and DR3 transgenic mice before (BCH) and after (ACH) they were cohoused. Pairwise Wilcoxon test was performed to obtain the statistical significance BCH and ACH for each DR3 and DR3.IL17$^{-/-}$ transgenic mice.

**Tables:**

**Table S1:** Differentially expressed gene list in the colon of DR3.IL17A$^{-/-}$ compared to DR3 transgenic mice calculated using *limma* package within *edgeR* in R. All 109 differentially expressed genes with *LogFC*>1.0 and *adj.p.val*<0.05 are shown.

| SN | Genes | logFC | AveExpr | t | P.Value | adj.P.Val |
|---|---|---|---|---|---|---|
| 1 | Eno1b | -12.154 | 1.443 | -19.576 | 0.000 | 0.000 |
| 2 | Hoxb13 | -11.448 | -1.890 | -19.897 | 0.000 | 0.000 |
| 3 | Hoxd13 | -9.589 | -1.902 | -10.871 | 0.000 | 0.000 |
| 4 | Casp14 | -8.793 | -1.658 | -13.128 | 0.000 | 0.000 |
| 5 | Glo1-ps | -8.601 | -0.491 | -9.588 | 0.000 | 0.000 |
| 6 | 2310079G19Rik | -8.148 | -2.842 | -8.433 | 0.000 | 0.000 |
| 7 | Rpl15-ps6 | -7.886 | 0.116 | -6.560 | 0.000 | 0.002 |
| 8 | Gm13237 | -7.823 | -0.170 | -8.445 | 0.000 | 0.000 |
| 9 | Ly6g | -7.548 | -2.237 | -11.113 | 0.000 | 0.000 |
| 10 | Tgm3 | -6.671 | 3.560 | -31.635 | 0.000 | 0.000 |
| 11 | Vtcn1 | -6.393 | -3.095 | -8.575 | 0.000 | 0.000 |
| 12 | Mettl7a2 | -6.307 | -3.303 | -8.664 | 0.000 | 0.000 |
| 13 | Igkv8-18 | -6.293 | -0.666 | -8.186 | 0.000 | 0.000 |
| 14 | Fxyd4 | -6.059 | -1.910 | -4.809 | 0.000 | 0.025 |
| 15 | 5033404E19Rik | -5.855 | -2.774 | -5.566 | 0.000 | 0.008 |
| 16 | Gm7334 | -5.659 | 1.342 | -5.672 | 0.000 | 0.007 |
| 17 | Sval1 | -5.631 | 3.704 | -19.493 | 0.000 | 0.000 |
| 18 | Evx2 | -5.587 | -2.795 | -6.518 | 0.000 | 0.002 |
| 19 | Gm8540 | -5.532 | -3.496 | -7.667 | 0.000 | 0.000 |
| 20 | Atp12a | -5.477 | 0.033 | -18.752 | 0.000 | 0.000 |
| 21 | Chit1 | -4.989 | -3.144 | -5.998 | 0.000 | 0.004 |
| 22 | Trpv6 | -4.912 | -0.557 | -8.873 | 0.000 | 0.000 |
| 23 | Igkv2-112 | -4.725 | 1.275 | -9.585 | 0.000 | 0.000 |
| 24 | Fut9 | -4.701 | -1.951 | -6.631 | 0.000 | 0.002 |
| 25 | Ighv7-1 | -4.595 | 0.648 | -6.919 | 0.000 | 0.001 |
| 26 | Ninj2 | -4.593 | -1.906 | -5.754 | 0.000 | 0.006 |
| 27 | St8sia5 | -4.551 | -1.819 | -5.220 | 0.000 | 0.013 |
| 28 | Ighv1-61 | -4.532 | 1.365 | -7.272 | 0.000 | 0.001 |
| 29 | Tmprss13 | -4.269 | -0.183 | -8.813 | 0.000 | 0.000 |
| 30 | Gjb5 | -4.261 | -1.541 | -4.778 | 0.000 | 0.025 |
| 31 | Hoxd12 | -4.259 | -3.247 | -4.345 | 0.000 | 0.049 |
| 32 | Vsig1 | -4.255 | -1.212 | -6.516 | 0.000 | 0.002 |
| 33 | Ighv10-3 | -4.253 | 3.640 | -11.518 | 0.000 | 0.000 |

| | | | | | | |
|---|---|---|---|---|---|---|
| 34 | B3gnt7 | -4.195 | 5.973 | -34.648 | 0.000 | 0.000 |
| 35 | Rpl15-ps2 | -3.829 | -0.635 | -4.963 | 0.000 | 0.019 |
| 36 | Itih2 | -3.817 | -1.521 | -4.471 | 0.000 | 0.041 |
| 37 | Mettl7a3 | -3.571 | -1.774 | -4.445 | 0.000 | 0.042 |
| 38 | Pla2g4f | -3.458 | 0.531 | -5.797 | 0.000 | 0.006 |
| 39 | Trpv3 | -3.403 | 3.252 | -12.943 | 0.000 | 0.000 |
| 40 | Thbs4 | -3.334 | 3.057 | -21.508 | 0.000 | 0.000 |
| 41 | Hoxa13 | -3.280 | -1.700 | -8.765 | 0.000 | 0.000 |
| 42 | Itln1 | -3.187 | 6.879 | -10.731 | 0.000 | 0.000 |
| 43 | Sycn | -3.151 | 2.937 | -24.593 | 0.000 | 0.000 |
| 44 | Nxpe4 | -3.057 | 3.610 | -15.040 | 0.000 | 0.000 |
| 45 | Insl5 | -2.941 | -1.314 | -6.488 | 0.000 | 0.002 |
| 46 | Ighv2-5 | -2.897 | 2.075 | -4.897 | 0.000 | 0.021 |
| 47 | Adgrf1 | -2.818 | 0.607 | -9.433 | 0.000 | 0.000 |
| 48 | Igkv3-4 | -2.711 | 3.280 | -8.454 | 0.000 | 0.000 |
| 49 | Igkv4-57 | -2.655 | 4.588 | -12.494 | 0.000 | 0.000 |
| 50 | Slc28a3 | -2.572 | 2.546 | -4.625 | 0.000 | 0.032 |
| 51 | Igkv4-68 | -2.565 | 4.316 | -8.356 | 0.000 | 0.000 |
| 52 | Pla2g2f | -2.494 | 3.879 | -7.097 | 0.000 | 0.001 |
| 53 | Ighv3-3 | -2.458 | 1.456 | -8.997 | 0.000 | 0.000 |
| 54 | Cyp2d12 | -2.407 | 1.294 | -9.324 | 0.000 | 0.000 |
| 55 | Best2 | -2.363 | 0.866 | -10.732 | 0.000 | 0.000 |
| 56 | Gm47283 | -2.290 | 5.085 | -10.117 | 0.000 | 0.000 |
| 57 | Adh1 | -2.274 | 5.559 | -21.681 | 0.000 | 0.000 |
| 58 | Ighv1-39 | -2.271 | 3.886 | -4.873 | 0.000 | 0.022 |
| 59 | Cyp2c68 | -2.248 | 4.529 | -8.006 | 0.000 | 0.000 |
| 60 | B3gnt5 | -2.203 | 3.517 | -6.569 | 0.000 | 0.002 |
| 61 | Ighv5-4 | -2.151 | 2.640 | -5.001 | 0.000 | 0.018 |
| 62 | Ggh | -2.100 | 5.137 | -16.144 | 0.000 | 0.000 |
| 63 | Cyp2d9 | -2.078 | 0.066 | -4.490 | 0.000 | 0.040 |
| 64 | Zfp791 | -2.041 | 2.587 | -4.591 | 0.000 | 0.034 |
| 65 | Slc15a2 | -2.026 | 2.158 | -4.924 | 0.000 | 0.020 |
| 66 | Nox1 | -2.008 | 3.528 | -7.361 | 0.000 | 0.001 |
| 67 | Nt5e | -1.973 | 5.284 | -10.629 | 0.000 | 0.000 |
| 68 | Duoxa2 | -1.952 | 6.303 | -10.058 | 0.000 | 0.000 |
| 69 | Ang4 | -1.951 | 7.834 | -9.720 | 0.000 | 0.000 |
| 70 | Ighv2-9-1 | -1.949 | 3.374 | -4.962 | 0.000 | 0.019 |
| 71 | Slc15a1 | -1.948 | 6.682 | -8.009 | 0.000 | 0.000 |
| 72 | Igkv3-5 | -1.942 | 3.424 | -5.541 | 0.000 | 0.008 |

| | | | | | | |
|---|---|---|---|---|---|---|
| 73 | Cldn8 | -1.909 | 4.312 | -9.203 | 0.000 | 0.000 |
| 74 | Eno3 | -1.762 | 3.750 | -6.374 | 0.000 | 0.002 |
| 75 | Clic6 | -1.762 | 3.833 | -5.762 | 0.000 | 0.006 |
| 76 | Cd177 | -1.749 | 6.807 | -16.983 | 0.000 | 0.000 |
| 77 | Adamts15 | -1.691 | 4.728 | -5.747 | 0.000 | 0.006 |
| 78 | Ccl28 | -1.628 | 7.068 | -12.416 | 0.000 | 0.000 |
| 79 | Igkv9-120 | -1.622 | 4.390 | -4.733 | 0.000 | 0.027 |
| 80 | Hoxa11 | -1.621 | 0.018 | -5.452 | 0.000 | 0.009 |
| 81 | Ceacam10 | -1.593 | 5.986 | -8.932 | 0.000 | 0.000 |
| 82 | Aqp4 | -1.573 | 6.556 | -14.118 | 0.000 | 0.000 |
| 83 | Saa1 | -1.550 | 7.353 | -7.683 | 0.000 | 0.000 |
| 84 | Ano1 | -1.550 | 3.699 | -6.163 | 0.000 | 0.003 |
| 85 | Tcf7l1 | -1.529 | 2.331 | -4.795 | 0.000 | 0.025 |
| 86 | Cela1 | -1.499 | 4.613 | -7.343 | 0.000 | 0.001 |
| 87 | Gm15401 | -1.437 | 3.493 | -4.550 | 0.000 | 0.036 |
| 88 | Prdx6 | -1.317 | 8.165 | -8.030 | 0.000 | 0.000 |
| 89 | Retnlb | -1.259 | 5.150 | -4.445 | 0.000 | 0.042 |
| 90 | Scd2 | -1.133 | 9.600 | -5.131 | 0.000 | 0.015 |
| 91 | Plin4 | 1.287 | 6.266 | 4.615 | 0.000 | 0.033 |
| 92 | Cyp4b1 | 1.379 | 4.923 | 4.760 | 0.000 | 0.026 |
| 93 | Slc13a1 | 1.393 | 7.159 | 5.688 | 0.000 | 0.006 |
| 94 | Hbb-bs | 1.412 | 5.567 | 5.082 | 0.000 | 0.016 |
| 95 | Naaladl1 | 1.451 | 8.878 | 5.901 | 0.000 | 0.005 |
| 96 | Oas2 | 1.473 | 3.640 | 4.420 | 0.000 | 0.044 |
| 97 | Tef | 1.533 | 4.008 | 5.337 | 0.000 | 0.011 |
| 98 | Oasl2 | 1.568 | 5.620 | 8.209 | 0.000 | 0.000 |
| 99 | Fabp4 | 1.636 | 8.267 | 8.666 | 0.000 | 0.000 |
| 100 | Ifit1 | 1.636 | 6.835 | 13.024 | 0.000 | 0.000 |
| 101 | Rpl3 | 1.638 | 7.213 | 9.483 | 0.000 | 0.000 |
| 102 | Thrsp | 1.641 | 5.122 | 4.949 | 0.000 | 0.020 |
| 103 | Ddx60 | 1.649 | 4.067 | 6.229 | 0.000 | 0.003 |
| 104 | Ifit3 | 1.670 | 4.893 | 6.902 | 0.000 | 0.001 |
| 105 | Retn | 1.716 | 4.432 | 5.022 | 0.000 | 0.018 |
| 106 | Sis | 1.727 | 7.589 | 5.489 | 0.000 | 0.009 |
| 107 | Igkv12-98 | 1.757 | 2.715 | 4.414 | 0.000 | 0.044 |
| 108 | Oas3 | 1.774 | 4.742 | 8.831 | 0.000 | 0.000 |
| 109 | Dbp | 1.855 | 4.802 | 9.977 | 0.000 | 0.000 |
| 110 | Rpl15 | 1.893 | 7.014 | 8.315 | 0.000 | 0.000 |
| 111 | Igkv14-100 | 1.910 | 3.744 | 5.128 | 0.000 | 0.015 |

| | | | | | | |
|---|---|---|---|---|---|---|
| 112 | Car3 | 2.300 | 7.529 | 24.744 | 0.000 | 0.000 |
| 113 | Cfd | 2.334 | 7.125 | 24.230 | 0.000 | 0.000 |
| 114 | Adipoq | 2.474 | 4.756 | 11.111 | 0.000 | 0.000 |
| 115 | Plin1 | 2.574 | 4.541 | 7.430 | 0.000 | 0.001 |
| 116 | Lgals2 | 2.688 | 5.834 | 6.063 | 0.000 | 0.004 |
| 117 | Tcaim | 2.984 | 2.326 | 6.378 | 0.000 | 0.002 |
| 118 | Trgc2 | 2.984 | 1.211 | 4.446 | 0.000 | 0.042 |
| 119 | Cyp2e1 | 3.009 | 5.145 | 15.014 | 0.000 | 0.000 |
| 120 | Lyrm7 | 3.114 | 0.716 | 4.632 | 0.000 | 0.032 |
| 121 | Gm16011 | 4.232 | -0.321 | 4.370 | 0.000 | 0.047 |
| 122 | Igkv14-126 | 5.013 | 0.842 | 7.976 | 0.000 | 0.000 |
| 123 | Cylc2 | 8.644 | -1.325 | 9.999 | 0.000 | 0.000 |

## References


1. S. K. Shahi, S. N. Freedman, R. A. Dahl, N. J. Karandikar, A. K. Mangalam, Scoring disease in an animal model of multiple sclerosis using a novel infrared-based automated activity-monitoring system. *Sci Rep* **9**, 19194 (2019).
2. A. F. Tyler, J. P. Mendoza, M. Firan, N. J. Karandikar, CD8(+) T Cells Are Required For Glatiramer Acetate Therapy in Autoimmune Demyelinating Disease. *PLoS One* **8**, e66772 (2013).
3. A. Mangalam *et al.*, HLA-DQ8 (DQB1*0302)-restricted Th17 cells exacerbate experimental autoimmune encephalomyelitis in HLA-DR3-transgenic mice. *J Immunol* **182**, 5131-5139 (2009).
4. A. K. Mangalam *et al.*, Absence of IFN-gamma increases brain pathology in experimental autoimmune encephalomyelitis-susceptible DRB1*0301.DQ8 HLA transgenic mice through secretion of proinflammatory cytokine IL-17 and induction of pathogenic monocytes/microglia into the central nervous system. *J Immunol* **193**, 4859-4870 (2014).
5. L. Goschl *et al.*, A T cell-specific deletion of HDAC1 protects against experimental autoimmune encephalomyelitis. *J Autoimmun* **86**, 51-61 (2018).
6. A. M. Thornton, E. M. Shevach, CD4+CD25+ immunoregulatory T cells suppress polyclonal T cell activation in vitro by inhibiting interleukin 2 production. *J Exp Med* **188**, 287-296 (1998).
7. F. Krueger, Trim Galore!: a wrapper tool around Cutadapt and FastQC to consistently apply quality and adapter trimming to FastQ files. (2014).
8. B. Langmead, S. L. Salzberg, Fast gapped-read alignment with Bowtie 2. *Nat Methods* **9**, 357-359 (2012).
9. F. Beghini *et al.*, Integrating taxonomic, functional, and strain-level profiling of diverse microbial communities with bioBakery 3. *Elife* **10**, (2021).
10. D. Li, C. M. Liu, R. Luo, K. Sadakane, T. W. Lam, MEGAHIT: an ultra-fast single-node solution for large and complex metagenomics assembly via succinct de Bruijn graph. *Bioinformatics* **31**, 1674-1676 (2015).
11. A. Mangalam *et al.*, Human Gut-Derived Commensal Bacteria Suppress CNS Inflammatory and Demyelinating Disease. *Cell Rep* **20**, 1269-1277 (2017).
12. S. Andrews. (2010).
13. N. L. Bray, H. Pimentel, P. Melsted, L. Pachter, Near-optimal probabilistic RNA-seq quantification. *Nat Biotechnol* **34**, 525-527 (2016).
14. R Core Team, R: A language and environment for statistical computing *R Foundation for Statistical Computing, Vienna, Austria*, (2020).
15. M. D. Robinson, D. J. McCarthy, G. K. Smyth, edgeR: a Bioconductor package for differential expression analysis of digital gene expression data. *Bioinformatics* **26**, 139-140 (2010).
16. S. X. Ge, D. Jung, R. Yao, ShinyGO: a graphical gene-set enrichment tool for animals and plants. *Bioinformatics* **36**, 2628-2629 (2020).